

Reply to reviewers

Reviewer #1

Page 1 line 14. 'high concentrations of chromophoric dissolved organic matter', why this matters?

Originally was suggested since CDOM may create a coating around the particle that is expected to enhance the light absorption per unit of weight. However, this effect is likely minor, thus this CDOM influence was deleted from the text

Page 3 line 20. How PIM and POM were estimated?

We expand the sentence as: 'The inorganic fraction of SPM (i.e., particulate inorganic matter or PIM) was obtained after removing the organic fraction (i.e., particulate organic matter or POM) of the original sample by combustion at 450°C for 6 h. Due to the dehydration of clays, this procedure may introduce an additional uncertainty of -10% and +10% on particulate inorganic (PIM) and organic matter (POM), respectively (Barillé-Boyer et al., 2003; Stavn et al., 2009)'.

Page 3 line 26, CDOM is the fraction below 0.2um typically. Here you seem to call any fraction passing a filter CDOM. Make sure people understand that or use a different name, for example filtered fractions.

We agree and clarify: 'CDOM is defined here as the fraction of dissolved organic matter passing through a membrane with a nominal pore size of 0.2 μm '.

Page 3 line 30, I believe this type of method has been used way before Rottgers.

**Yes, the 'flat method' it was originally proposed by Bricaud and Stramski (1990)
The reference was added**

What did you hope to achieve with a baseline correction (e.g. Zaneveld et al.,)?

This is a first order correction for scattering effects on non-water absorption coefficient estimates.

Is it reasonable to assume scattering is spectrally flat?

It is an assumption and there is debate. Some studies have reported a spectral dependency on volume scattering functions or particulate backscattering ratios (Chami et al., 2006; McKee et al., 2009; McKee et al., 2013). But there is doubt regarding if this assumption can be generalized (McKee et al., 2013).

Why did you choose this scattering correction (e.g. as opposed to the proportional or Rottgers one)? **We are aware that other methods exist (e.g., proportional to wavelength, Monte Carlo) (Zaneveld et al., 1994; McKee et al., 2013). However, the performance of these techniques to correct for residual scattering is not satisfactory either and/or may require additional optical information that we didn't have during the field surveys (e.g., particulate backscattering ratio) (McKee et al., 2013).**

Also we say, 'Thus, the calculation of particulate absorption coefficients is expected to have a bias with respect to true values measured using absorption-meter instruments that are less influenced by particulate scattering (e.g., point-source integrating-cavity absorption meters) (Röttgers et al., 2014).

Page 4 line 20. It looks like you are using something similar to Gordon's formulation (replacing bb with b). Why not do it from the get go and skip equations (1) and (2)?

These optical proxies were deleted and no need to make reference to Gordon's formulation. We work now with two optical proxies commonly used in the literature, γ and $Svis$.

Page 4 line 25, $aspm(\lambda_6)/aspm(\lambda_4)$ This is basically an indicator for [Chl]. You will get a better one by doing a line-height subtraction.

BOI indexes are not longer part of the manuscript

Page 4 Line 26. you may want to look Boss et al., 2004, JGR & 2009, LOM, for the use of $a(676)$ -line height/ $c(660)$ for particulate composition.

Thanks for the advice. We checked two indices of particle composition suggested in Boss et al. (2004) JGR and Boss et al. (2009) LOM. The first index relates bb/c to POC/SPM and the second index relates bbp/bp to chlorophyll concentration/cp. Although very interesting, these two proxies were not evaluated since no backscattering measurements were obtained during our surveys.

Page 4 Line 29. Don't forget you have the spectral-slope of beam attenuation to work with as well

Yes, we are aware of relationships between the spectral slope of cp and the hyperbolic slope of the particle size distribution (Boss et al., 2001). Additional correlations of cp spectral slope values were included as part of the analysis

Page 5 line 1, 'it will be very useful for an optical oceanographer evaluating your result if they could see figures of the SPECTRA of the mass normalized IOPs.

We added one additional figure (fig 2) where averaged ap^* and bp^* for the whole study area and each subregion are shown as a function of wavelength are shown

Page 5 Line 5, 'why not also compute c^* for which there is a longer literature?' **Although it is possible and interesting, our main interest is focused in IOPs that separate scattering from absorption effects. This is not the case for c or cp , thus their use makes interpretation of optical processes less clear.**

Page 5 line 12, 'you may want to refer to it as the exponent of the power-law distribution. Junge is usually used to denote the one with a differential exponent of 4'

Done

Page 5 line 16, 'you can use D50 from the LISST as a more robust parameter'
Additional correlations between parameter D50 (here symbolized with D_m), spectral slope of particulate beam attenuation (γ), differential slope particle size distribution (ξ), mass fraction of PIM or concentration of PIM/concentration of SPM ratio (F_{SPM}^{PIM}), and mass-specific optical coefficients did not show a general improvement with respect to parameter γ (see below). The correlation will depend on the size fraction

Correlations in the following table are based on 23 sampling locations.

	F_{SPM}^{PIM}	D_m	γ	ξ
$F_{SPM}^{0.2 - 0.4 \mu m}$	-0.42*	-0.51*	0.53*	-0.28 **
$F_{SPM}^{0.4 - 0.7 \mu m}$	0.35	0.41 *	-0.43*	0.11 *
$F_{SPM}^{0.7 - 10 \mu m}$	0.23	0.08	-0.38*	0.12 *
$F_{SPM}^{>10 \mu m}$	-0.08	0.21	0.13	-0.04

Page 7 line 1, 'your paper is totally lacking an uncertainty analysis. You need to add uncertainties in all your calculated values based on:replication. Assumptions (e.g. scattering correction used, finite acceptance angle of the ac-9)'.

One additional section 4.1 was included in discussion to summarize the different uncertainties involved in measuring IOPs. There was not replication of discrete samples, however it was possible to compute the optical variability during the ac-s measurements. This information is described in discussion along with the assumptions regarding the transmissometer and the scattering effects on a estimates.

Page 7 line 16, 'not having backscattering measurements and radiometry, this is a hard case to make.'

We agree , we talk now about optical proxies instead of remote sensing proxies

Page 8 line 22, 'But note that multiple scattering may have affected their optical measurements'

We added this observation to the discussion. 'Notice that part of this decrease can be attributed to an incomplete removal of multiple scattering effects'.

Page 8 line 24, 'This is known for a long while, e.g. Morel's 1974 work'

We added this reference

Page 8 line 31, 'CDOM cannot explain increase in a_SPM*'

The effect of CDOM on ap* was not quantified and is likely to be minor, thus it is a weak statement. Thus it was deleted from the text

Page 9 line 12, 'this will be true for in-situ aggregates (Slade's work). However, you are disrupting aggregates, so it is less likely'

We clarify the sentence as follows:

'Since particle aggregates were altered during our experiments, the influence of particle density on mass-specific optical coefficients cannot be quantified as this effect is mainly observed in undisrupted marine aggregates (Slade et al. 2011..'

Reviewer #2

General comments

In sum, this paper requires a massive reanalysis of the data and a massive effort at rewriting.

The corrected version of the manuscript was totally re-structured, many sections rewritten, new figures, new analysis of data and deletion of redundant tables

Specific Comments:

Page 1, lines 7-9. The language in this manuscript can be pretty cryptic. Some expansion is required here and below for clarity even though I realize abstracts are supposed to be kept as short as possible. Suggested wording: Abstract. Empirical mass-specific absorption (aSPM *) and scattering (bSPM*) coefficients of suspended particulate matter (SPM) were measured for different size fractions (proposed to be 0.2-0.4 μm , 0.4-0.7 μm , 0.7-10 μm , and >10 μm) in the surface waters (0-5 m depth) of the Saint Lawrence Estuary and Saguenay Fjords (SLE-SF) during the spring of 2013. True optical absorption and scattering cross sections were determined for the total PIM and POM, in addition to mass-specific absorption and scattering coefficients.

The abstract was rewritten and we talk now about true optical absorption and scattering cross sections

Page 1, line 10. A synopsis of the results of the determination of the true optical absorption cross sections also needs to be reported here. It requires pulling together the results on the spectral range of absorption cross sections of at least PIM to document the effects of adsorbed iron on clay minerals or suspended iron oxides in the PIM. That is, an analysis of the true absorption cross section, a_j , for chemical fraction j , organic or inorganic. The true optical cross sections determined here provide the information to interpret the empirical coefficient ratios reported for size fractionation, etc. This information documents the statements in the final sentence of the abstract such as for the effects of chemical composition and absorption variability on what is reported here.

Spectral changes on aspm* are now reported and discussed in terms of iron effects on particulate absorption.

Page 1, lines 13-14. It is not at all clear here what the authors mean when identifying variability of the empirical mass-specific absorption and scattering coefficients. In addition, the results of this study call into question the utility and feasibility of utilizing these empirical coefficient ratios.

Suggested wording: Gironde River). aSPM * ... particulates. Correlation analysis of the optical properties and the empirical ratios of this study suggests that particle composition has the most significant impact on variability of aSPM * and particle size distribution has the most significant impact on bSPM* variability. The fact that knowledge of the optical cross sections is necessary to interpret these empirical ratios calls into question the utility of aSPM * and bSPM* in general models of microphysical and biogeochemical processes proposed for all coastal/estuarine systems.

The abstract was rewritten and results clarified

A fundamental problem with all correlational analyses, as opposed to a well-defined regression analysis, is the fact that correlational analysis merely records the cooccurrence of phenomena without postulating a fundamental relationship between variables of the phenomena. High correlations simply mean that other, more fundamental relationships may be causing the co-occurrence of unrelated phenomena. An analysis based on aSPM * and bSPM* will always be correlational and limited to the specific region where the relationships were defined.

Like any other statistical analysis there are pros and cons. A well-defined regression analysis has many and strict assumptions that should be met such as normal distribution of variables, random sampling, etc. This issue is absent when non-parametric correlations are used

Yes, we are always talking about our study area regarding correlations results

Page 2, lines 1-2. Algorithms based only on CSPM will never have the accuracy required for optical inversions because SPM is undefined optically, an unknown mixture of inorganic and organic matter. Therefore partition of SPM into at least major chemical composition classes (PIM and POM) and estimation of size distribution are required independently for optically-based remote sensing algorithms of primary productivity and suspended mineral dynamics of “disappearing shorelines” etc.

It is a relative questioning. Depends on the level of accuracy you are interested. Many studies have been proposed for estimating CSPM based on remote sensing methods. Adding remotely sensed PIM and POM to calculate SPM will also have a large error due to the addition of two errors linked to PIM and POM algorithms

Page 2, lines 13-17. A fundamental issue here, not often discussed in the literature but should be, is consideration of what constitutes Inherent Optical Properties and how this concept should be applied to the measurements taken in the field. One can take a bulk absorption or scattering coefficient of an undefined mixture of material suspended in water and easily determine their mass-specific coefficients but what do they really mean? The absorption coefficient of dissolved matter such as CDOM can be related to a general

chemical class of dissolved compounds and we can come up with a measurement of absorption that can be related by refractive index or whatever to a similar group of compounds and the absorption coefficient of CDOM can be analyzed in a quantitative manner. That is, an absorption coefficient of CDOM from one region can be related quantitatively (absorption cross section, etc.) to an absorption coefficient of CDOM from an entirely different region. So an absorption coefficient of CDOM can be called an optical property as per the definition of Bohren and Huffman (1983, p. 227), "There are two sets of quantities that are often used to describe optical properties: the real and imaginary parts of the complex refractive index $N = n + ik$ and the real and imaginary parts of the complex dielectric function (or relative permittivity) $\epsilon = \epsilon' + i\epsilon''$." In other words, genuine optical properties must have defined complex refractive indices and permittivities which the absorption and scattering coefficients of SPM do not have. Again, SPM is an unknown mixture of both mineral and organic matter and the SPM composition varies from point to point in the same region and furthermore varies between different regions. If we separate out mineral and organic matter we can approach true optical properties of this material by having more narrowly defined complex refractive indices and relative permittivities. By this definition the absorption and scattering coefficients of SPM cannot be called optical properties and their mass-specific versions, a_{SPM}^* and b_{SPM}^* , should only be called empirical mass-specific ratios. At best the absorption and scattering coefficients of unpartitioned SPM can be referred to as "optical proxies." Thus the term "optical properties" should be limited to the optical cross sections and absorption and scattering coefficients for PIM and POM only. This rationale will be followed in my subsequent comments.

I understand your point and thank you for your wonderful insight but we try to go along with definitions of optical properties currently used in the current literature. This should be a good topic for another publication.

Page 3, lines 15-20. The description of the procedures utilized here is confusing. The process of sizefractionation of suspended matter in water is tricky (Sheldon and Sutcliffe, 1969; Sheldon, 1972). It is important to recognize the difference between screens and filters as was pointed out by Sheldon and Sutcliffe (1969). A screen is designed for separation of materials in suspension of a particular diameter and a filter is designed for retention of all materials in suspension greater than a given diameter. That is, the manufacturer guarantees that a filter of a given nominal pore size will retain all material larger than the nominal pore size. However, as a filter slowly gets clogged it will retain material smaller than the nominal pore size. All the filters mentioned in this section were not designed to be screens and the nominal manufacturer's pore size is not the median pore size for retention as demonstrated by Johnson and Wangersky (1985), Sheldon (1972), and Sheldon and Sutcliffe (1969). The median size of particles retained is a function of the volume of sample filtered and the concentration of particles in the sample. The use of manufacturer's nominal pore size to delineate the size fractionation, as is done in this paper, does not correctly give the limits of the size fractions unless the authors did extensive tests on the particle size-range and retention capacity of the filters they utilized under their particular conditions of filtration. It is not clear which filter was used for the loss-on-ignition

determination of the total suspended mass and partitioning of it into PIM and POM. If the Whatman GF/F filter were used for SPM, PIM, and POM determination then why was the same filter used for fractionation into the supposed 0.4-0.7 and 0.7-10 mm size ranges? The Whatman GF/F filter can work well for removing nearly all particles down to about 0.2 mm out of suspension. Chavez et al. (1995) reported about 95% particle retention down to 0.2 mm by Whatman GF/F filters. Johnson and Wangersky (1985) derived a theory, involving diffusion and adsorption of suspended materials and filter pore walls, demonstrating that filters will retain particles much smaller than the nominal pore size reported by the manufacturer. One of their conclusions was that a Whatman GF/C filter of nominal pore size 1.2 mm, depending on concentration of materials in suspension and flow rate of filtration, could be an efficient method of separating out materials in suspension larger than 0.7 mm

No, different filters were used in this study to fractionate 0.4-0.7 and 0.7-10 micron fractions

This sentence was clarified as:

Size fractionation of SPM into four size classes (>10 μm , 0.7-10 μm , 0.4-0.7 μm , and 0.2-0.4 μm) was done after sequentially filtering the original samples through pre-weighted membranes having a diameter of 47 mm and a pore size of 10 μm (Whatman, polycarbonate), 0.7 μm (GF/F, Whatman, glass fiber), 0.4 μm (Whatman, polycarbonate), and 0.2 μm (Nucleopore, polycarbonate), respectively.

Also, we add the whatman GF/F was used for PIM and POM determinations.

We wrote: The mass of PIM was obtained after removing the organic fraction (i.e., POM) from the total mass of SPM as computed for CSPM determinations. The mass of POM was eliminated by combustion of GF/F filters at 450°C and during 6 h. The concentration of POM was calculated as the difference between the dry mass of SPM and the dry mass of PIM. The precision of PIM determinations was 25% since an additional variability of 10% was added to the error measurement of SPM mass due to the dehydration

We are aware of the issues using the nominal pore size and the retention of small particulates. We mention that issue when computing mass-specific optical coefficients in discussion

The authors need to give a table of the suspended masses retrieved by the various filter sizes and compare it with the total mass retrieved on a single filter. Given the fact that the nominal pore sizes of the filters do not correspond to the actual sizes of material retained on the filters, I would be surprised if the masses of the sub samples from various filters added up to the total mass retrieved from one filter.

Since the masses retained by the filters are the key to the results reported in this paper, I suggest some sort of optimization scheme to adjust the total mass and the sum of the subsample masses so that a probable mass partition can be utilized based on the masses retained on the filters, i.e. adjusting the various masses to sum up to the total mass filtered. This would presumably require various weighting factors to be applied to the measured masses. It appears the Whatman GF/F filters were used for both total mass filtration and for determining two sub-sample ranges. The authors must explain carefully just how this was accomplished.

Good point. Total mass of SPM was calculated based on gravimetric determinations based on 0.7 microns GF/F filters. This is standard in the literature (Stavn and Richter, 2008; Rottger et al, 2014). However, it is true that $aspm^*$ and $bspm^*$ are overestimated since $aspm$ and $bspm$ are based on particulates above 0.2 microns. This is due to the pre-filtration of samples through nucleopore membranes in order to remove CDOM+seawater contributions.

In the other hand, size fractions of IOPs correspond to the same size fractions of mass. Thus, there should be no bias on mass-specific coefficients of IOPs for SPM.

To evaluate the effect of sieving on retaining smaller particulates than pore size, comparison were made between filtered samples without pre-sieving vs sum of size-fractioned samples. In average, adding mass fractions resulted in a total mass difference for particulates larger 0.7 microns of +31.4%. In other words, a 31.4% overestimation of mass for >0.7 microns particulates when the sum of weights of fractions is performed rather than weighting the unfractionated sample

These filter ‘effects’ on retained SPM mass may be possible to correct as the example described above. However, we didn’t filter total unfiltered samples through 0.2 or 0.4 microns membranes since we did sequential filtering. Thus, factors such as sum fractions mass/unfiltered mass for size fractions >0.2 or >0.4 microns could not be calculated in our study.

In discussion, we described the general overestimation of $aspm^*$ and $bspm^*$ values and ‘filter effects’ on mass-specific properties of size fractions of SPM

Page 3, lines 22-23. The authors point out that they did not use the correction factors discussed by Barille-Boyer et al. (2003) to account for the loss of structural water by the suspended clay minerals. The authors state that an error of about 10% will accrue to the PIM and POM estimates if ignored. The 10% error is only for the inorganics while the 10% error in inorganic mass will generate a greater error in the organic mass, easily as much as 30% overestimation error in the POM estimate. I suggest the authors utilize the extensive geochemical publications on the St. Lawrence Estuary to estimate the probable concentration of the various clay mineral species in their samples in order to calculate this error. One possible source is Danglejan and Smith (1973).

**We added to the text the larger error of POM mass determinations
By using the Danglejan and Smith (1973) data related to clay composition in the
SLE, we calculated an underestimation of PIM mass of 3.1%
Also, 3.22% of loss of ignition PIM must be removed from POM in order to obtain a
POM mass corrected by structural water of clays**

**Based on Barillé-Boyer et al. (2003) factors and clay composition data obtained in
the Saint Lawrence Estuary (D'Anglejan and Smith, 1973), the estimated error of
PIM determinations due to dehydration of clays was 3.1%. Thus, PIM mass
determinations has a maximum uncertainty of 18.1%. Notice that error in POM
mass estimates is slightly greater than that associated to PIM mass (18.22% of loss
on ignition PIM mass**

Page 3, line 30. The weightings used to correct the mass fractionation of the filters should be applied here to the estimates of spectral absorption by the various estimated size fractions.

See above the issue of using this weighting for certain size fractions

Page 4, lines 4-5. The spectral measurements of c should also be adjusted by the weightings for the SPM size fractions as mentioned above for the absorption coefficient. Of course this then results in weighted values of b for the size fractions. Then one should check this with the known optical relation that the various b values measured for the sub fractions should add up to the b value recorded for the total SPM. All of this information about a and b values should be recorded in a table.

**Actually IOPs after each filtration are not added up but are decreasing in
magnitude as samples are filtered through membranes having a smaller pore size
New figures are shown for size fractions of $aspm^*$ and $bspm^*$. For some samples,
the calculation of IOPs lead to negative values at some wavelengths. These curves
are not included as part of the plots and might be related to issues linked to the
filters or particle aggregation/disaggregation effects**

Page 4, lines 5-7. The authors mention the use of a LISST-100X for determining particle size spectra in the range 3-170 mm and then never mention these data again. If the data were important they should be brought into the discussion, especially considering the lack of precision and accuracy in the attempt to do size fractionation of suspended matter in this study. Were the LISST data used to estimate the Junge slope g ? If so the extensive analysis of submicron materials in this study will not have relevance to g and these correlations must be removed from the analysis. If the LISST-100X data were not used then the use of the LISST-100X is irrelevant to this study and should not be mentioned.

**Yes, LISST-100x was an important instrument to compute differential Junge slope.
More interpretation and results and included now regarding ξ**

We don't think correlations between smaller than 2 microns particulates and ξ are spurious since it is feasible correlations due to the fact than smaller than 2 microns optics is correlated with greater than 2 microns optics. We verified that possibility.

Page 4, lines 15-30. This section is totally obscure as many relationships are brought in that do not directly reflect on the studies proposed here and may have some relevance to the material at hand but I am hard put to find relationships or relevancies. The introductory material introduces the Morel and Prieur (1977) formulas for estimating Rrs that depend on measurements of backscattering bb which, however, are not used in this study. Further on, the equations (1) and (2) are supposedly used to derive Eqs. (3) – (5), the biogeo-optical (BOI) indices which do not utilize bb . Clearly, the reader requires a derivation of how one gets from a backscattering formulation to a scattering formulation. The BOI indices are proposed to estimate changes in bulk chemical composition and size distribution of SPM. From these formulas of BOI indices to the end of the page the argument becomes increasingly obscure and hard to follow. It would help to write the variables used in the manuscript into fractions created by a math editor rather than the plethora of inline fractions. The inline fractions contribute to the obscurity of the argument. The relation between formulations with backscattering to derive formulations with total scattering have to be laid out clearly. The BOI for “size 1” and “size 2” have to be explained clearly. Does this refer to all the size fractionations attempted here or to just one or two? If so, whichsize fractions? Where does the polynomial function F come in and how do we get this from the derivation of Eqs. (4) and (5)? What is the relevance of Gordon's (1988) formulation for Rrs, in terms of bb and Eqs. (4) and (5) in terms of b? Again, the reader has to be led carefully from a backscattering formulation to a total scattering formulation. This section requires expansion and a total rewrite.

All this section was rewritten and BOI indexes were removed and replaced by traditional indexes used in the literature (spectral slope of particulate beam attenuation and mass-specific particulate absorption coefficient within the visible spectrum).

Part of decision of eliminating BOI indexes was the lack of bb measurements.

Page 5, line 3. Utilizing empirical relations involving POC (essentially the CO₂ from ashed organic matter) generalized to POM is difficult in marine systems because the crude relations between POC and POM are based on chemical analysis of detritus from higher plants. The relation between the two variables is not straightforward in marine systems because the organic content of phytoplankton differs in quantity and quality from higher plants and the various groups of phytoplankton, diatoms and prochlorophytes for example, differ from each other. I always recommend coupling POC data with POM data because of this difficulty. So relations coupling aSPM(l), CSPM, and POC become increasingly problematic and definitely region-specific. The derivation of the BOIsize indices for particle size being based on the unknown spectral slope of backscattering also becomes problematic. For that matter, there is still controversy about whether there actually is a spectral slope associated with the backscattering coefficient. These indices along with BOIcomp may be of some empirical use but they will always be regionally

limited without independent information on chemical composition and size distribution to interpret them. The problem with the indices proposed here and similar indices proposed elsewhere is that they are qualitative in nature. At best, ignoring all the problems, one can only come up with qualitative “greater than or lesser than” estimates of size or chemical composition without any quantitative information which is what is needed for valid and accurate predictions of particle and biogeochemical dynamics.

We agree with the reviewer. BOI indexes are no longer part of the manuscript

Page 5, line 9. Since the empirical mass normalizations reported here do not fit the Bohren and Huffman definition of optical properties, I suggest the following, **2.6 Optical cross sections and massnormalized coefficients, and the substitution of “optical coefficients or mass-specific ratios”** throughout the manuscript when the term “IOP” is used to refer to the empirical mass-normalized coefficients or absorption and scattering coefficients determined for SPM.

Done

Hopefully well understood. Replacing whenever IOP is present

Page 5, lines 10-11. The mass-specific absorption and scattering cross sections were estimated with Model I multiple regression. Just as Model II regression was used elsewhere in this paper, Model II multiple regression must be used for the best estimates of the mass-specific cross sections (s). The only time that Model I regressions can be used in place of Model II regressions is with a high R² value between the proposed dependent and independent variables, say R² > 0.95. That is not the case here. It is my experience that the best estimate of slopes (as used to estimate s values) with R² values as low as reported here is definitely with Model II multiple regression (Stavn and Richter, 2008; Richter and Stavn, 2014).

Sorry, model II was missing from the text. Now was added and it means that response and independent variables have a random error

Optical cross sections for chemical fractions of SPM were calculated based on **multiple regression model II analysis (i.e., independent and response variables have random errors)** (Sokal et al., 1995; Stavn and Richter, 2008):

$$Y = \beta_1 [CPIM] + \beta_2 [CPOM]$$

Page 5, line 12. In light of above I suggest in this line the replacement of “optical property” with “optical coefficient.”

done

Page 5, line 16. As suggested earlier, the masses used for calculating the mass-specific absorption and scattering coefficients of size-fractionated SPM should be optimized and weighted for these calculations.

As mentioned before, this is not possible for all size fractions

Page 5, lines 23-25. Although the slope of the power-law formulation is often used to describe the particle size distribution (PSD), the actual PSD's for estuarine systems as reported previously (Risović, 2002; Zhang et al. 2014; Zhang et al. 2017) should be mentioned. The power-law distribution is a firstorder approximation of the PSD for particles greater than about 2 mm diameter. Therefore it will often work for total scattering with calculations involving only particles in the 2 mm + range. It fails for submicron particles and since assertions are made for size fractions less than 2 mm diameter, the use of this assumption becomes questionable. Again, the use of the g slope gives a qualitative feeling for a relative distribution of large and small particles in suspension but fails when quantitative relations are desired.

This is especially true of backscattering estimates as demonstrated by Risović (2002) and there seem to be analogies being made for parameters proposed and used in this paper that are based on backscattering. The bottom line again is a development here that is qualitative at best and regionally limited.

I guess you mean The power-law distribution is a firstorder approximation of the PSD for particles greater than about 2 mm diameter, **greater than 2 microns, right?**

We included in methods the limitations of using Junge slope vs Risovic

‘Although particle size distribution in natural waters may not follow a Junge-type slope, its use here was justified since our main interest was to have a first-order assessment of size effects of particulates on optical coefficient’s variability’.

Indeed, the calculation of ξ is only valid for particulates greater than 2 μm . A more realistic representation of PSD is the model proposed by Risovic (2002). This parameterization mainly includes two particle populations (‘large’ and ‘small’) having different refractive index and was applied for the first time in littoral environments by Stavn and Richter (2008). Thus, relationships between ξ and optical coefficients in this study are local and should not be generalized to other littoral environments.

Page 5, lines 25-27. It is important to keep in mind here that the SPM parameters proposed and the SPM relations utilized in this paper are only useful when correlated with actual determinations of chemical species and some independent estimation of the size-classes of PSD. The authors claim that functionalities between “IOP’s” and BOI indices were investigated with linear regression analyses. However, I see no report of regression coefficients in the data tables, only correlation coefficients.

BOI indexes are not apart of the manuscript anymore. We do correlations not linear regressions

Page 6, lines 7-11. How were the g slope's calculated? Were they from the masses of the various size sub-ranges or from the LISST data? This is important because of the rampant inconsistencies between the size fraction masses and the g slope estimates. The mode of calculation must be delineated and the data shown in a table to be able to evaluate what is reported here. Even though the largest mass of 0.2-0.4 mm particles is reported for the LE the smallest g slope is reported for this region. The 90% error for the g coefficient, for which the area is not delineated here, is strong evidence for the inability of the Junge-type slope to describe, even qualitatively, the PSD patterns for this study. A table is required for the g slopes and their errors.

Error and range of ξ values was added to the manuscript. Also, a detailed calculation of ξ is included

Page 8, lines 7-9. Even if the n value is low for correlations between the BOI indices and the optical cross sections, this is the only way to validate the BOI indices and the correlations should be given with proper caveats.

In Discussion we highlighted the limitations of the reduced number of samples when correlating optical proxies

'Also, the reduced number of sampling locations and the geographic variability of ξ - γ relationships were additional factors likely explaining the lack of a general functionality for the study area'

Page 8, line 10. The Discussion section, in general, reads too much like a Results section. We should assume that the relevant statistical relations are in the results section and here we are interested only in the overall pattern of the results and the explanation of the patterns laid out in the results section.

**The discussion was improved with results regarding iron and new optical proxies
Comparison of our mass-specific optical coefficients and optical cross sections with those in the literature is a common procedure of discussing results in most publications**

Page 9, lines 22-23. The assertion here is that a larger portion of large particles and lower g slope's (how were they calculated?) were found in the LE region. Yet Table 2 indicates that parts of the LE region had the greatest contribution of 0.2-0.4 mm particles and a contribution of particles greater than 10 mm equivalent to or less than that of SF and UE. Here is an obvious problem with the g slope. The interpretation that these large particles may have been organic in nature contributes to the uncertainty of the interpretation of the SPM-based coefficients and measurements advocated in this paper.

The calculation of the slope ξ is described in methods. Yes, there is a lot spatial variability on ξ but lower ξ values were measured in LE waters. We found a general inverse correlation between CPIM/CSPM and ξ ($\rho_s = -0.41$, $P = 0.049$) for

the study area and suggesting that relatively large particulates have an organic origin. This relationship was intensified in LE waters ($\rho_s = -0.58$, $P = 0.022$).

Page 10, lines 16-17. Table 4 is nearly incomprehensible. The extensions of the table without the columns being identified is what makes the table incomprehensible. And again, in this section the statistical tests should be in the results section and we are interested only in the interpretations of the patterns in the results. The correlation coefficients reported in the table are low even though presumably significant. Again, if g were determined from the LISST data then any analysis of submicron particles and g is simply invalid.

The first column of the table was labeled. More statistical detailed were added to the text. Now is table 2. It is true that no correlations should be expected between ξ and mass-specific optical coefficients of size fraction 0.2-0.4 and 0.4-0.7 microns cause the LISST limitations regarding submicrometric particles. However, correlations may exist due to dependencies between size fractions. In other words, $aspm^*$ of 0.2-0.4 and 0.4-0.7 microns are correlated with $aspm^*$ of 0.7-10 and >10 microns For the case of $bspm^*$, no significant correlations were computed for 0.2-0.4 and 0.4-0.7 microns.

Page 10, lines 24-25. The theoretical calculations of Babin et al. (2003) assumed the Junge slope g when estimating particle concentrations and calculating the Mie scattering based on the particle concentrations predicted by the Junge slope. Since the PSD has been demonstrated to not be Jungian (Risović, 2002; Zhang et al. 2014; Zhang et al. 2017), especially in coastal waters, the Babin et al. (2003) results are not relevant here.

Table 4 does not show any relationship between $bspm^*$ and g , i.e. g is not in the table at all. This closest approach is apparently in Table A1. Here we see that the correlations of the optical coefficients of nominal size fractions of SPM and g vary all over the map, from positive to negative, significant and non-significant, not at all supporting the hypothesis of g being a significant and explanatory variable in the this analysis. This also falsifies the hypothesis that absorption coefficients and ratios are parameters of use in general models of the occurrence and dynamics of suspended matter.

The sentence about Babin et al. (2003) was deleted in discussion

Page 11, lines 2-4. Again, the empirical indices proposed in this paper are poorly described and defined. What do the superscripts “size 1” and “size 2” mean? The BOI indices may be of some utility but again, like all similar indices based on empirical coefficients of total SPM, they are strictly qualitative in nature. The unknowns in the bulk coefficients in their definition will always cast doubt on their interpretation if ancillary evidence on PSD and composition are not available.

BOI indexes are not anymore part of the manuscript

Page 11, lines 20-21. Suggested wording: These relationships will be useful in investigating local and regionally-limited relationships and properties of SPM. Without separate independent studies of true optical properties of PIM and POM, and of PSD, these relationships will remain problematical.

We added the first sentence to the end of the conclusions paragraph

Technical Corrections:

Page 2, line 5. Bowers et al. (2009) reported estimates of mass-specific scattering coefficients of and biogeo-physical characteristics of PIM, not SPM.

Ok corrected

Page 6, line 26. Replace “properties” with “coefficients.”

done

Page 9, lines 9-10. The English usage here is nearly incomprehensible. Correct this and similar constructions with a native speaker of English.

Done

Pages 19-30. The tables presented here are nearly impossible to interpret. The table extensions to multiple pages have incomplete columns and no captions to the columns. The table captions are limited and cryptic.

Many tables were removed to simplify content. Also, more labels were added to identify columns

References:

Bohren, C.H. and D.R. Huffman. 1983. Absorption and Scattering of Light by Small Particles. John Wiley and sons, New York. Xiv + 530 pp.

Chavez, F.P., Buck, K.R., Bidigare, R.R., Karl, D.M., Hebel, D., Latasa, M., and Campbell, L. 1995. On the chlorophyll a retention properties of glass-fiber GF/F filters. Limnol. Oceanogr., 40: 428–433.

Johnson, B. D. and P. J. Wangersky. 1985. Seawater filtration: Particle flow and impaction considerations. Limnol. Oceanogr. 30: 966-971, doi:10.4319/lo.1985.30.5.0966.

Richter, S.J. and R.H. Stavn. 2014. Determining functional relations in multivariate oceanographic systems: Model II multiple linear regression. Journal of Atmospheric and Oceanic Technology, 31:

1663-1672.

Risović, D. 2002. Effect of suspended particulate-size distribution on the backscattering ratio in the remote sensing of seawater. *Appl. Opt.*, 41(33): 7092-7101.

Sheldon, R.W. 1972. Size separation of marine seston by membrane and glass-fiber filters. *Limnol. Oceanogr.*, 17(6): 494-498.

Sheldon, R.W. and W.H. Sutcliffe, Jr. 1969. Retention of marine particles by screens and filters. *Limnol. Oceanogr.*, 14(3): 441-444.

Zhang, X., Stavn, R.H., Falster, A.U., Rick, J.J., Gray, D. and R.W. Gould, Jr. 2017. Size distributions of coastal ocean suspended particulate inorganic matter: Amorphous silica and clay minerals and their dynamics. *Estuarine, Coastal and Shelf Science*. DOI: 10.1016/j.ecss.2017.03.025

Optical properties of size and chemical fractions of suspended particulate matter in littoral waters of Québec

Gholamreza Mohammadpour¹, Jean-Pierre Gagné¹, Pierre Larouche², Martin A. Montes-Hugo^{1*}

¹Institut des Sciences de la Mer de Rimouski, 310 Allée des Ursulines, Office P-216, Rimouski, Québec, Canada, G5L 3A1

²Institut Maurice-Lamontagne, Pêches et Océans Canada, Mont-Joli, Québec, Canada, G5H 3Z4

Correspondence to: Martin A. Montes-Hugo (martinalejandro_montes@uqar.ca)

Abstract. ~~Mass specific absorption (a_{SPM}^*) and scattering (b_{SPM}^*) coefficients of suspended particulate matter (SPM) were measured for different size (0.2-0.4 μm , 0.4-0.7 μm , 0.7-10 μm , and >10 μm) and chemical (organic vs mineral rich) fractions in surface waters (i.e., 0-5 m depth) of the Saint Lawrence Estuary and Saguenay Fjords (SLE-SF) during spring of 2013. Empirical mass-specific absorption (a_{SPM}^*) and scattering (b_{SPM}^*) coefficients of suspended particulate matter (SPM) were measured for four size fractions (i = 0.2-0.4 μm , 0.4-0.7 μm , 0.7-10 μm , and >10 μm) in surface waters (i.e., 0-5 m depth) of the Saint Lawrence Estuary and Saguenay Fjords (SLE-SF) and during June of 2013. True absorption (σ_a) and scattering (σ_s) cross sections for total particulate inorganic (PIM) and organic (POM) matter were also measured. Lastly, the response of two optical proxies (the spectral slope of particulate beam attenuation coefficient and mass-specific particulate absorption coefficient, hereafter γ and $Svis$, respectively) to changes on particle size and chemical composition was examined. For the spectral range 400-700 nm, scattering cross sections for particulate inorganic matter were commonly larger with respect to those measured in other littoral environments. This phenomenon was attributed the lower water turbidity and associated decrease on mean particle size of SLE-SF surface waters with respect to other river influenced regions (e.g., Gironde River). a_{SPM}^* values in our study area were relatively high in locations having iron enriched particulates. Lastly, correlation analysis suggests that particle composition (size distribution) has a larger impact on a_{SPM}^* (b_{SPM}^*) variability. For the spectral range 400-700 nm, relatively low a_{SPM}^* values (i.e., 0.01-0.02 $\text{m}^2 \text{ g}^{-1}$) indicate large-sized particle assemblages with relatively high particulate organic carbon and chlorophyll a per unit of mass. Conversely, largest a_{SPM}^* values (i.e., > 0.5 $\text{m}^2 \text{ g}^{-1}$) corresponded with locations having relatively small-sized or mineral-rich particulates. Particle-associated iron likely explained the relatively high a_{SPM}^* (440) values in low-salinity environments of SF. The differential Junge slope of particle size distribution had a larger correlation with b_i^* (Spearman rank correlation coefficient ρ_s up to 0.37) with respect to a_i^* (ρ_s up to 0.32). Conversely, the ratio between PIM and SPM concentration had a stronger influence on a_i^* (ρ_s up to 0.50). Size spectrum (chemical composition) of SPM appears to be more important affecting relatively large (small) particulates. The magnitude of γ was sensitive to changes on size fractions of SPM mass. In LE~~

locations, the magnitude of S_{vis} was directly correlated with the mineral content of SPM. This may indicate a potential association between iron and inorganic enrichment of particles in areas of the estuary with a larger marine influence.

1 Introduction

The distribution of suspended particulate matter (SPM) in coastal and estuarine environments has a major influence on several biogeochemical processes (e.g., phytoplankton blooms) (Guinder et al., 2009), ecosystem structure (e.g., food webs) (Dalu et al., 2016) and dispersion of pollutants (e.g., copper, mercury, polycyclic aromatic hydrocarbons) (Ma et al., 2002; Ramalhosa et al., 2005; Tremblay et al., 2005). The concentration of SPM (C_{SPM}) is an important variable for estimating primary productivity (Devlin et al., 2008) and modeling thermodynamic processes (Löptien and Meier, 2011) due to its influence on underwater light attenuation (Morel and Antoine, 1994). Light absorption by suspended particulates is essential for several photochemical processes related to the carbon cycle (e.g. photosynthesis, production of dissolved inorganic and organic carbon) (Estapa et al., 2012). Lastly, the concentration of SPM (CSPM) (Table 1) is an important variable for modeling thermodynamic processes and computing heat budgets (Löptien and Meier, 2011) due to its influence on underwater light attenuation (Morel and Antoine, 1994; Devlin et al., 2008).

Formatted: English (U.S.)

Remote sensing allows mapping of SPM in littoral environments where the spatial and temporal variability of suspended particulates is relatively high. Indeed, synoptic measurements derived from spaceborne ocean color sensors are commonly applied for estimating C_{SPM} based on visible (i.e., wavelength, $\lambda = 400\text{-}700$ nm) (Miller and McKee, 2004; Montes-Hugo and Mohammadpour, 2012) and NIR-SWIR (near-and short-wave infrared) ($\lambda = 700\text{-}3,000$ nm) (Doxaran et al., 2002) spectral bands. Despite this progress, there is still a lack of understanding regarding how SPM microphysical characteristics (e.g., particle chemical composition and size distribution) relate to mass-specific inherent optical properties (HOPs) coefficients. This knowledge is essential for deriving more accurate remote sensing algorithms for estimating C_{SPM} and developing new optical inversions for retrieving second-order attributes of SPM (i.e., chemical composition, size distribution).

The remote sensing of particle size and/or composition in coastal and oceanic waters has been attempted based on four main methodologies: (1) analysis of spectral changes of IOPs (Loisel et al., 2006), (2) empirical relationships between mass-specific IOPs and biogeo physical characteristics of SPM (e.g. mean diameter of particulates) (Bowers et al., 2009), (3) optical inversions of different volume scattering functions (Zhang et al., 2014), and (4) changes on water leaving polarized reflectance (Loisel et al., 2008).

The optical characterization of particle size distribution (PSD) and/or composition in coastal and oceanic waters has been attempted based on four main methodologies: (1) analysis of spectral changes of inherent optical properties (Boss et al., 2001; Loisel et al., 2006), (2) empirical relationships between mass-specific optical cross sections and biogeo-physical characteristics of particulate inorganic matter (PIM) (e.g., mean diameter) (Bowers et al., 2009) and SPM (e.g. apparent density of particulates) (Neukermans et al., 2012), (3) optical inversions of different volume scattering functions (Zhang et

al., 2014), and (4) changes on water leaving polarized reflectance (Loisel et al., 2008). A widely used methodology for estimating particle size spectra changes is the use of the spectral slope of particulate beam attenuation coefficient (γ) due to its relationship with the differential Junge slope of particle size distribution (ξ) (Boss et al., 2001).

5 Lastly, the biogeo-optical modeling of size and chemical fractions of SPM has a major scientific interest for understanding the dynamics of different mineral iron forms in coastal waters (Estapa et al., 2012) as particle-associated iron has two specific light absorption bands (wavelength, $\lambda = 360\text{-}390$ nm and $\lambda = 400\text{-}450$ nm). Also, Estapa et al. (2012) demonstrated that optical proxies such as the spectral slope of particulate absorption (S_{vis}) within the visible spectral range ($\lambda = 400\text{-}700$ nm) could be used for estimating dithionite-extractable iron and organic carbon content in marine samples. Iron can be part of organic (e.g., complexed forms) or inorganic (e.g., silicate sheets) particulates having a broad size range (e.g., from clays to amorphous aggregates) (Bettoli et al., 2008). Thus, the analysis of different fractions of SPM is essential for understanding the complex fate of iron in aquatic systems. Linking iron distributions with optical properties of size and chemical fractions of SPM may allow the development of proxies for mapping iron based on optical (in water and remote sensing) measurements. This is particularly advantageous for long-term monitoring projects as direct iron measurements are very expensive, difficult, and demand highly trained technicians.

10 15 The Saint Lawrence Estuary (SLE) and the Saguenay Fjords (SF) constitute a large sub-Arctic system characterized by relatively high concentrations of chromophoric dissolved organic matter (CDOM) (Nieke et al., 1997). The accurate monitoring of C_{SPM} and SPM characteristics in these waters is crucial for understanding regional climate effects on coastal erosion (Bernatchez and Dubois, 2004) and occurrence of harmful algae blooms (Fauchot et al. 2008). Accurate remote sensing measurements of CSPM and SPM microphysical characteristics in these waters is crucial for understanding regional 20 25 climate effects on coastal erosion (Bernatchez and Dubois, 2004) and occurrence of harmful algae blooms (Fauchot et al. 2008). Despite this need, there is a lack of information regarding how optical properties are linked to particle second order attributes and what is the spatial variability of mass specific IOPs of SPM. For this reason, our contribution has two main objectives: (1) to characterize the mass normalized IOPs for size and chemical fractions of SPM in different locations of the SLE SF and during spring conditions, and (2) to establish relationships between mass specific optical properties of SPM, 'bulk' particle characteristics related to size distribution and mineral content, and optical proxies within the visible and near-infrared spectral range (i.e., $\lambda = 700\text{-}1,000$ nm). However, in order to accomplish this task it is essential to know how mass-specific optical coefficients of suspended particulates are influenced by particle composition and size distribution changes. To our knowledge, mass-specific absorption and scattering coefficients of SPM size fractions have never been reported in 30 the literature even though it has a practical application in biogeo-optical inversions and biogeochemical studies regarding the dynamics of trace metals.

This study is organized in three sections. In the first section, mass normalized spectral absorption and scattering coefficients for size and chemical SPM fractions are calculated for different optical environments of the SLE SF that are characterized by

5 a variable CDOM contribution to light attenuation and distinct particle assemblages. In the second section, the response of mass normalized absorption and scattering coefficients of SPM fractions to variations in particle size distribution and mineral content are investigated. Lastly in the third section, covariations between optical proxies and microphysical properties of SPM are examined.

10 This study is organized in three sections. In the first section, a_{SPM}^* , b_{SPM}^* , σ_a and σ_b coefficients are calculated for different optical environments of the SLE-SF that are characterized by a variable CDOM contribution to light attenuation and distinct particle assemblages. In the second section, the response of mass-specific optical coefficients and optical cross sections of SPM fractions to variations in PSD and mineral-content of suspended particulates is investigated. Lastly in the third section, the influence of PSD and mineral enrichment of particulates on γ and $Svis$ is examined. Also, spatial distributions $Svis$ are interpreted in terms of salinity changes and potential particulate iron-rich environments.

2 Data and methods

2.1 Study area

The SLE can be divided in two main regions having contrasting biological productivity and bathymetry: the upper (UE) and the lower (LE) estuary (Levasseur et al., 1984). Non-algal particulates (NAP) and CDOM dominate the underwater light

15 attenuation of UE waters (Nieke et al., 1997). This is in part related to the inflow of CDOM-rich and NAP-rich waters coming from the St. Lawrence River (Tremblay and Gagné, 2007). Unlike NAP and CDOM, contribution of phytoplankton to IOPs increases towards the mouth of the SLE (Montes Hugo and Mohammadpour, 2012) to inherent optical properties increases towards the mouth of the SLE (Montes-Hugo and Mohammadpour, 2012; Xie et al., 2012). The study of optical properties in SLE waters began during the late 80's. Babin et al. (1993) investigated the horizontal variability of the specific absorption coefficient of phytoplankton (i.e., absorption coefficient normalized by concentration of chlorophyll + phaeopigments) in surface waters during summer of 1989 and 1990. During the summer of 1990, Nieke et al. (1997) studied the spatial variability of CDOM in terms of fluorescence and absorption spectra. Also, this study reported for the first time relatively high (up to 3 m^{-1}) particulate beam attenuation coefficients (c_{SPM}) and inverse relationships between salinity, c_{SPM} , and CDOM absorption coefficients (a_{CDOM}). Larouche and Boyer-Villemaire (2010) proposed remote sensing models for estimating PIM in SLE and Gulf of Saint Lawrence regions. Xie et al. (2012) showed inverse relationships between salinity and absorption coefficients of non-algal particulates and highlighted the extremely high a_{CDOM} values (i.e., up to 5.8 m^{-1} at $\lambda = 412 \text{ nm}$) along the Saguenay Fjord.

20 -Historical studies performed during summer of 1975 suggest that size distribution of SPM differs between UE, LE and SF regions (Poulet et al., 1986). Based on surface samples, Poulet et al. (1986) found a dominance of relatively 'small-sized' (i.e., mode diameter $< 10 \text{ } \mu\text{m}$) and 'large-sized' (i.e., $> 30 \text{ } \mu\text{m}$) particulates over the UE and the mouth of the SLE, respectively. Conversely, the remaining locations of the LE were characterized by particulates having an intermediate size (i.e., $8-40 \text{ } \mu\text{m}$). In surface waters of SF, SPM is mainly composed by very small particles (i.e., $2-3 \text{ } \mu\text{m}$) during spring months

(Chanut and Poulet, 1979). However, this pattern is reversed during autumn. Several investigations point out that suspended particulates in SLE-SF regions are principally composed by inorganic matter (D'Anglejan, and Smith, 1973; Larouche and Boyer-Villemaire, 2010). This mineral contribution varies between 60 and 95% of dry weight depending on location and period of the year (Yeats, 1988; Larouche and Boyer-Villemaire, 2010). 5 Despite their important contribution, none of these studies reported mass-normalized optical coefficients for different size or chemical fractions of SPM nor an assessment of particle composition and size distribution effects on a_{SPM}^* , b_{SPM}^* , and optical cross sections of PIM and POM.

2.2 Field surveys

Discrete water samples for biogeochemical and optical measurements were obtained in 23 locations distributed throughout the SLE ($n = 18$) and SF ($n = 5$) regions (Fig. 1). 10 One discrete sample was obtained in each sampling locations but in site 6 where 2 measurements were made during June 3 and 6 of 2013. Samples corresponding to a sampling depth of 0-2 m were collected during June 3-9 of 2013 by using an oceanographic rosette equipped with Niskin bottles (volume = 12 L). For each sampling location, mass of different size fractions of SPM, 15 IOPs for different SPM size fractions, and particle size distribution spectra were measured, optical coefficients for different SPM size fractions, and particle size distribution spectra were measured inside the wet lab of the vessel.

2.3 Biogeochemical analysis

20 The concentration of SPM and particulate inorganic matter (C_{PIM}) in g m^{-3} was measured gravimetrically with a precision of $\pm 15\%$ and 25% , respectively (Mohammadpour et al., 2015). The concentration of SPM (CSPM) in g m^{-3} was measured gravimetrically after filtering a volume of seawater through pre-weighed GF/F filters (47 mm, average pore size = $0.7 \mu\text{m}$, Whatman). The precision of CSPM determinations was 15% (Mohammadpour et al., 2015). The precision of 15% was computed as the percentage of ± 1 standard deviation with respect to the arithmetic average of weight corresponding to 10 replicas. Size fractionation of SPM was done after sequentially filtering the original samples through pre-weighed membranes having a diameter of 47 mm and a pore size of $10 \mu\text{m}$ (Whatman, polycarbonate), $0.7 \mu\text{m}$ (GF/F, Whatman, glass fiber), $0.4 \mu\text{m}$ (Whatman, polycarbonate), and $0.2 \mu\text{m}$ (Nucleopore, polycarbonate). Size fractionation of SPM into 25 four size classes ($>10 \mu\text{m}$, $0.7-10 \mu\text{m}$, $0.4-0.7 \mu\text{m}$, and $0.2-0.4 \mu\text{m}$) was done after sequentially filtering the original samples through pre-weighed membranes having a diameter of 47 mm and a pore size of $10 \mu\text{m}$ (Whatman, polycarbonate), $0.7 \mu\text{m}$ (GF/F, Whatman, glass fiber), $0.4 \mu\text{m}$ (Whatman, polycarbonate), and $0.2 \mu\text{m}$ (Nucleopore, polycarbonate), respectively. The contribution of size fraction i to the total mass of SPM (F_{SPM}^i , $i = 0.2-0.4 \mu\text{m}$, $0.4-0.7 \mu\text{m}$, $0.7-10 \mu\text{m}$, and $>10 \mu\text{m}$) was 30 computed by normalizing their weight by the total weight of unfractioned samples that were retained on $0.2 \mu\text{m}$ membranes weight by the sum of weights corresponding to the 4 size fractions i . The inorganic fraction of SPM (i.e., particulate inorganic matter or PIM) was obtained after removing the organic fraction (i.e., particulate organic matter or

POM) of the original sample by combustion at 450°C for 6 h. Due to the dehydration of clays, this procedure may introduce an additional uncertainty of 10% and +10% on particulate inorganic (PIM) and organic matter (POM), respectively (Barillé-Boyer et al., 2003; Stavn et al., 2009). The mass of PIM was obtained after removing the organic fraction (i.e., POM) from the total mass of SPM as computed for CSPM determinations. The mass of POM was eliminated by combustion of GF/F filters at 450°C and during 6 h. The concentration of POM was calculated as the difference between the dry mass of SPM and the dry mass of PIM. Based on Barillé-Boyer et al. (2003) factors and clay composition data obtained in the Saint Lawrence Estuary (D'Anglejan and Smith, 1973), the estimated error of PIM determinations due to dehydration of clays was 3.1%. Thus, PIM mass determinations has a maximum uncertainty of 18.1%. Notice that error in POM mass estimates is slightly greater than that associated to PIM mass (18.22% of loss on ignition PIM mass). The contribution PIM and POM to SPM mass is F_{SPM}^j where j superscript symbolizes PIM or POM, respectively.

2.4 Optical measurements

Discrete water samples for CDOM absorption coefficient (a_{CDOM}) determinations were done in the lab following protocols suggested by Müller and Horn (1990). CDOM is defined here as the fraction of dissolved organic matter passing through a membrane with a nominal pore size of 0.2 μm . Total absorption (a) and beam attenuation (c) coefficient measurements of four size fractioned water samples (0.2–0.4 μm , 0.4–0.7 μm , 0.7–10 μm , and >10 μm) were performed onboard using an absorption beam attenuation meter (ac-s, WetLabs). Optical measurements were corrected by applying a flat baseline at a reference wavelength of 715 nm (Bricaud and Stramski, 1990). Total absorption (a) and beam attenuation (c) coefficient measurements were done on unfiltered and size-fractioned filtered water samples previously described in section 2.3. Discrete samples for optical coefficients were measured onboard by using an absorption-beam attenuation meter (ac-s, WetLabs, $\lambda = 400.3\text{--}747.5\text{ nm}$, average spectral resolution = 4 nm, path-length = 10 cm, accuracy $\pm 0.001\text{ m}^{-1}$). In order to minimize the presence of bubbles, a pump (ISMATEC MCP-Z) was used to gently circulate the samples through the ac-s tubes. Spikes on raw signal associated to bubbles were removed by visual inspection. Residual scattering on absorption measurements was removed by applying a flat baseline at a reference wavelength of 715 nm (Bricaud and Stramski, 1990). This is a first order correction for scattering effects on non-water absorption coefficient estimates. Thus, the calculation of particulate absorption coefficients in this study is expected to have a bias with respect to true values measured using absorption meter instruments that are less influenced by particulate scattering (e.g., point-source integrating cavity absorption meters) (Röttgers et al., 2014). Spectral scattering coefficient measurements (b) were derived by subtracting a from c at each wavelength. This is a first order correction for scattering effects on non-water absorption coefficient estimates. Thus, the calculation of particulate absorption coefficients in this study is expected to have a bias with respect to true values measured using absorption-meter instruments that are less influenced by particulate scattering (e.g., point-source integrating-cavity absorption meters) (Röttgers et al., 2013). Lastly, values of a and c were corrected by water temperature and salinity variations (Pegau et al. 1997). Spectral values of a_{SPM} were derived by subtracting a_{CDOM} and the absorption coefficient for seawater (a_w) to a at each wavelength. The contributions $a_{CDOM} + a_w$ were measured by using the a -tube (i.e.,

reflective tube) of the ac-s and after pre-filtration of total samples through a membrane having a pore size of 0.2 μm (nucleopore, Whatman). CDOM is defined here as the fraction of dissolved organic matter passing through a membrane with a nominal pore size of 0.2 μm . Similar to a_{SPM} calculations, the magnitude c_{SPM} was computed after subtracting CDOM and seawater contributions to c as derived by using the c -tube (i.e., opaque tube) of the ac-s instrument. Lastly, particulate scattering coefficients (b_{SPM}) were derived by subtracting a_{SPM} to c_{SPM} values.

5 The particle size spectra within the size range 3–170 μm were measured on ‘bulk’ (i.e., without size fractionation) samples and by using a red laser (wavelength = 670 nm) diffractometer (LISST-100X, type B, Sequoia Scientifics) (Agrawal et al. 1991).

10 The particle size spectra within the size range 3–170 μm were measured on ‘bulk’ (i.e., without size fractionation) samples and by using a red laser (wavelength = 670 nm) diffractometer (LISST-100X, type B, Sequoia Scientifics) (Agrawal et al. 1991). LISST bench determinations were discrete and performed on board of the ship. Lab measurements were performed by using a chamber and a magnetic stir bar in order to homogenize the samples and avoid sinking of particulates. The optical path was covered with a black cloth to minimize ambient light contamination during the scattering measurements. The 15 LISST-100X instrument can measure 32 scattering angles within an angular range of 0.08–13.5°, thus, particulates with a diameter between 1.25 and 250 μm can be quantified. However only the interval 3–170 μm was analyzed due to variability of particle shape and refractive index in the first bins (i.e., < 3.2 μm) (Agrawal et al., 2008; Andrews et al., 2010), stray light effects in the first bins (Reynolds et al. 2010), and bias related to particle sinking in the last bin (i.e., 170–250 μm) (Reynolds et al. 2010). Measurements were made during a period of 3 minutes at 1 Hz, and resulting raw data were quality controlled 20 by using the Hampel filter algorithm for eliminating outliers (Pearson, 2005). The number of particles per unit of volume within each size class ($N(D)$) was computed by dividing the particle volume concentration ($V(D)$) by the diameter (D) of a volume-equivalent sphere for the midpoint of each individual class:

$$N(D) = 6 V(D) (\pi D^3)^{-1} \quad (1)$$

25 A total of 25 particle size bins were calculated based on inversions of the scattering pattern and by applying an inversion kernel matrix derived from scattering patterns of spherical homogenous particles as predicted from Mie theory and a realistic range of index of refraction. The particle size distribution ($N'(D)$) was defined as the average number of particles within a given size class of width ΔD and per unit of volume (Reynolds et al., 2010):

$$N'(D) = N(D) \Delta D^{-1} \quad (2)$$

The parameter ξ was computed as the exponent of the following power-type function:

$$N'(D) = N'(D_0) (D/D_0)^{-\xi} \quad (3)$$

30 where D_0 is the reference particle diameter and was set to 35.17 μm . Calculations of ξ were done by least square minimization of log-transformed data (Reynolds et al., 2010). Although particle size distribution in natural waters may not follow a Junge-type slope, its use here was justified since our main interest was to have a first-order assessment of size effects of particulates on optical coefficient's variability. Indeed, the definition of ξ based on LISST measurements applies

for particulates greater than 2 μm . A more realistic representation of PSD is the model proposed by Risovic (1993). This parameterization mainly includes two particle populations ('large' and 'small') having different refractive index and has been recently applied in littoral environments by different studies (Zhang et al., 2013; Zhang et al., 2014; Zhang et al., 2017). Thus, relationships between ξ and optical coefficients in this study are local and should not be generalized to other littoral environments.

5

2.5 Optical proxies of particle microphysical characteristics

Optical composite parameters directly related to remote sensing reflectance (R_{rs}) (Table 1) were constructed based on *in-water* IOPs determinations. Unfortunately, no remote sensing reflectance measurements were available during this study. Spectral values of a and b can be linked to the irradiance ratio measured just below the water surface ($R(0')$) (Morel and Prieur, 1977):

$$R(0') = f \cdot b \cdot b_b^{\text{eff}} / a \quad (1)$$

$$R_{rs} = R(0') \cdot \kappa / Q_s(0') \quad (2)$$

where f is a coefficient that varies with atmospheric (e.g., solar zenith angle) and water (e.g., single scattering albedo) parameters (Morel and Gentilli, 1996), b_b^{eff} is the total (i.e., water + particulates) backscattering efficiency (i.e., b_b / b) where b_b is the total backscattering coefficient. The magnitude of κ depends on refraction and internal reflection of photons at the air-water interface. For a nadir looking sensor, the $Q_s(0')$ is defined as the ratio between upwelling irradiance and upwelling radiance just beneath the sea surface and as a function of the solar zenith angle (θ_0). From equations (1) and (2), three biogeo-optical indices (BOI) were proposed for estimating changes in 'bulk' chemical composition (superscript comp) and size distribution (superscripts size1 and size2) of SPM:

$$\text{BOI}^{\text{comp}} = \alpha_{\text{SPM}}(\lambda_6) / \alpha_{\text{SPM}}(\lambda_4) \quad (3)$$

$$\text{BOI}^{\text{size1}} = F((b(\lambda_1) \cdot a(\lambda_2)) \cdot (a(\lambda_1) \cdot b(\lambda_2))^\perp) \quad (4)$$

$$\text{BOI}^{\text{size2}} = F((b(\lambda_3) \cdot a(\lambda_4)) \cdot (a(\lambda_3) \cdot b(\lambda_4))^\perp) \quad (5)$$

where α_{SPM} is the particulate absorption coefficient, F is the polynomial function $g + g^2$, where $g = b(\lambda) \cdot (b(\lambda) + a(\lambda))^\perp$. Notice that F resembles Gordon's formulation of R_{rs} for nadir view geometry and optically deep water ($R_{rs} = \sum_{i=1}^2 f_i \cdot (b_b \cdot (a + b_b)^\perp)^\perp$) (Gordon et al., 1988), where $f_1 \approx 0.0949$ I and $f_2 \approx 0.0794$ I, $I \approx t^2 \cdot n^2$ or the air-sea interface divergence factor (t is the air-sea transmittance and n is the refractive index of seawater). $\lambda_1, \lambda_2, \lambda_3, \lambda_4, \lambda_5$ and λ_6 correspond to wavelengths 443, 488, 555, 570, 670 and 675 nm, respectively. Values of α_{SPM} were derived by subtracting the contributions of CDOM and seawater to a . The absorption coefficient (a_w) and scattering (b_w) coefficient of seawater were computed at *in situ* salinity and temperature by using empirical parameterizations suggested by Pope and Fry (1997) and Zhang et al. (2009), respectively.

The equation (3) was suggested based on empirical relationships between $a_{SPM}(\lambda_0)/a_{SPM}(\lambda_4)$ and POC/C_{SPM} ratios, where POC is the particulate organic carbon concentration (Wozniak et al., 2010). BOF^{size1} and BOF^{size2} indices for particle size distribution were based on Carder et al. (2004) and D'Sa et al. (2007) published R_{vs} band ratios, respectively. These ratios are correlated to the spectral slope of particulate backscattering. In general, BOF^{size} values are expected to increase as SPM becomes richer in POC. Likewise, BOF^{size1} and BOF^{size2} are anticipated to decrease as particulates become larger or water contribution to backscattering increases at relatively low water turbidities.

The parameter γ is positively correlated with the exponent of the particle number size distribution ($\xi = \gamma + 3 - 0.5 e^{-6\gamma}$, Boss et al., 2001) and negatively related with the mean particle size for particles smaller than 20 μm . The parameter γ was derived as the exponent of a power-type regression model of c_{SPM} as a function of wavelength:

$$c_{SPM}(\lambda) = c_{SPM}(488) (\lambda/\lambda_r)^{-\gamma} \quad (4)$$

where $\lambda_r = 488 \text{ nm}$ and it is the reference wavelength (Boss et al., 2013).

The magnitude of S_{vis} is positively correlated with extractable iron from crystalline and amorphous iron oxides and organic-iron complexes in measurements corresponding to marine samples (Estapa et al., 2012). Also for the same environments, S_{vis} is expected to covary in a direct way with the organic carbon content of particulates (Estapa et al., 2012).

The spectral slope of empirical mass-specific a_{SPM} coefficients (S_{vis}) was calculated by nonlinear fitting of a single-exponential decay function over the visible range 400-700 nm:

$$a_{SPM}^*(\lambda) = A e^{S_{vis}(\lambda-400)} + B \quad (5)$$

where the term B corresponds to an offset at near-IR wavelengths to account for nonzero absorption by mineral particles (Babin et al. 2003; Röttgers et al., 2014).

2.6 Optical cross sections and mass-normalized IOPs

Spectral values of mass-specific absorption (σ_a^j) and scattering (σ_b^j) cross sections for mineral and organic fractions of SPM were estimated from multiple regression analysis (Sokal et al., 1995), were estimated statistically by partitioning each optical coefficient with respect to the concentration of PIM and POM in each sample (see section 2.7). The superscript j indicates inorganic (PIM) or organic (POM) particulate matter. The superscript j indicates PIM or POM chemical fractions. For the case of size fractions of SPM, a mass-normalized optical property was calculated for particulate absorption and scattering coefficients:

$$a_i^*(\lambda) = a_i(\lambda) (m_i)^{-1} \quad (6)$$

$$b_i^*(\lambda) = b_i(\lambda) (m_i)^{-1} \quad (7)$$

where m is the mass in g m^{-3} for each size class i .

2.7 Statistical analysis

The influence of particle size and chemical composition variations on a_{SPM} , b_{SPM} , σ_a , σ_b , a_i^* , and b_i^* was investigated using the non-parametric Spearman rank correlation coefficient (ρ_s) (Spearman, 1904). This metric was also applied to examine the response of a_i^* and b_i^* values to changes on the exponent of the power law distribution of particle size distribution (γ) or the slope of log transformed number of particulates per unit of volume as a function of their size range (Junge, 1963). Values of γ were computed based on linear regression models where dependent and independent variables are randomly selected (i.e., type II parameterization). Although particle size distribution in natural waters may not follow a Junge type slope, its use here was justified since our main interest was to have a first order assessment of size effects of particulates on IOPs variability. The sensitivity of BOI^{comp} , BOI^{size1} , and BOI^{size2} to variations of different chemical and SPM size fractions was quantified based on the magnitude of ρ_s . Lastly, potential functionalities between mass normalized IOPs and BOI indices were examined for different study areas based on linear regression analysis model type II.

Optical cross sections for chemical fractions of SPM were calculated based on multiple regression model II analysis (i.e., independent and response variables have random errors) (Sokal et al., 1995; Stavn and Richter, 2008):

$$Y = \beta_1 [CPIM] + \beta_2 [CPOM] \quad (8)$$

where Y is the response variable representing a specific optical coefficient for unfractionated SPM, β_1 and β_2 are partial regression coefficients that correspond with σ^{PIM} and σ^{POM} , respectively. CPIM and CPOM are the concentrations of PIM and POM, respectively, in g m^{-3} .

The influence of particle size and chemical composition variations on mass-normalized optical coefficients of particulates (a_i^* , b_i^* , σ_a , σ_b) and optical proxies (γ and $Svis$) was investigated based on correlations with respect to ξ and F_{SPM}^{PIM} variables, respectively. In all cases, the intensity and sign of correlations were quantified based on non-parametric Spearman rank coefficient (ρ_s) (Spearman, 1904).

3 Results

3.1 Spatial variability of SPM fractions Spatial variability of microphysical properties of SPM

In terms of particle size distribution, contrasting areas in the SLE-SF were identified. In UE, particulates having a diameter larger than $10 \mu\text{m}$ had in average a contribution of 11% to the total SPM mass (Table 2). This proportion was lower in the LE (up to 9%) and SF (up to 6%) sub-regions. The largest mass contribution of smallest-sized particulates (i.e., diameter $< 0.4 \mu\text{m}$) was calculated in the lower estuary. This proportion was lower in the LE ($F_{SPM}^{>10 \mu\text{m}} = 0.01\text{-}0.11$) and SF (0.03-0.15) sub-regions. The largest mass contribution of smallest-sized particulates (i.e., diameter $< 0.4 \mu\text{m}$) was calculated in the lower estuary ($F_{SPM}^{0.2 - 0.4 \mu\text{m}} = 0.02\text{-}0.27$). Lastly, the intermediate size class $0.7\text{-}10 \mu\text{m}$ was the fraction having the maximum contribution to SPM in the SF (76.5% in average). Lastly, the intermediate size classes $0.4\text{-}0.7 \mu\text{m}$ and $0.7\text{-}10 \mu\text{m}$ were in average the fractions having the largest mass contributions to SPM in SF locations (0.01-0.14 and 0.66-0.87, respectively).

In general, the Junge slope calculations suggested the presence of relatively larger particulates in the LE with respect to UE and SF sub-regions. relatively larger particulates in the LE (arithmetic average \pm standard deviation = 3.28 ± 0.38 , N = 15) with respect to UE (3.46 ± 0.36 , N = 3) and SF (3.42 ± 0.39 , N = 5) sub-regions. Indeed, the arithmetic average and range of γ for LE, UE and SF locations were 1.67 and 0.9–2.4, 2.4 and 2.3–2.4, and 2.4 and 2.1–2.6, respectively. The uncertainty of γ calculations varied between 8 and 90% with smaller errors in the LE. The uncertainty of ξ calculations, as estimated from 2 standard errors, varied between 1.6 and 10.2% with smaller errors in the LE. Unlike particle size distribution, chemical composition of SPM was less variable (F_{SPM}^{PIM} range = 20 - 87 %). In average for each sub-region under investigation, the mass of suspended particulates was always dominated by inorganic matter (arithmetic average of F_{SPM}^{PIM} = 0.58, 0.62 and 0.70 for SF, UE and LE, respectively, Table 2). The largest variability of mineral content of SPM was characteristic of waters with relatively shallow depths and a greater contribution of freshwater discharge by the St. Lawrence River (e.g., sampling locations 12 and 13 in the UE, Fig. 1). In average, particle composition in UE, SF and LE sub-regions was dominated by minerals (F_{SPM}^{PIM} = 0.65 ± 0.13 , 0.67 ± 0.14 and 0.67 ± 0.14 for SF, UE and LE, respectively).

3.2 Relationships between SPM fractions and IOPs

In general, size and chemical composition of SPM were important second order attributes affecting the scattering coefficient of suspended particulates. In general, b_{SPM} response to changes on SPM size fractions and chemical composition (p_s up to 0.71 and 0.59, t up to 21.17 and 15.35, Student t test, respectively) was greater with respect to that associated to a_{SPM} (p_s up to 0.53 and 0.21, t up to 13.13 and 4.51, respectively, Student t test) (Table 3). The larger influence of particle size distribution on b_{SPM} compared to a_{SPM} values was supported by correlations between γ and IOPs (p_s up to 0.50, t up to 12.12, Student t test; p_s up to 0.33, t up to 7.34, Student t test) (Table A1). Unlike particle size, the impact of SPM chemical composition on a_{SPM} was principally manifested at relatively short wavelengths (i.e., $\lambda = 440$ –556 nm, p_s up to 0.21, t up to 4.51, Student t test, Table 3). Indeed, the highest correlations between SPM size fractions and a_{SPM} values were computed in the red-NIR spectral regions (e.g., p_s up to 0.41, t up to 9.44, Student t test).

3.3 Mass-specific optical properties of SPM Mass-specific optical coefficients of SPM

The variation of mass normalized scattering and absorption coefficients of SPM for different size and chemical fractions are shown in Fig. 2. Full spectral variation of regional averaged a_{SPM}^{\pm} and b_{SPM}^{\pm} values are depicted in Fig. A1 (Appendix A). In general, sub regional averages of mass normalized IOPs of particulates with different size ranges were higher with respect to optical cross sections of chemical fractions (up to 2 and 3 orders of magnitude for a and b , respectively). For a wavelength of 556 nm and over the whole study area, the range of values for $a_{0.2-0.4 \mu m}^{\pm}$, $a_{>10 \mu m}^{\pm}$, σ_a^{PIM} and σ_a^{POM} was 0.11 – 2.14 , 0.18 – 1.20 , 0.01 – 1.06 and 0.01 – $1.03 \text{ m}^2 \text{ g}^{-1}$, respectively (Fig. 2a). Likewise, for the same wavelength, the range of $b_{0.2-0.4 \mu m}^{\pm}$, $b_{>10 \mu m}^{\pm}$, σ_b^{PIM} and σ_b^{POM} was 1.82 – 2.39 , 1.05 – 1.49 , 0.03 – 1.06 and 0.03 – $0.36 \text{ m}^2 \text{ g}^{-1}$, respectively (Fig. 2b).

For the spectral range 440–556 nm, mass normalized absorption coefficients of SPM tended to be higher for particulates within the lower size range (i.e., 0.2–0.4 μm) (Fig. 2a, left axis). Also, this trend appeared to be reversed at longer wavelengths. Unlike mass normalized absorption coefficients of size fractions, mass specific cross sections of chemical fractions showed only differences within the red and near IR wavelengths (Fig. 2a, right axis). For the whole study area, the arithmetic average of mass normalized scattering coefficients for the size fraction 0.2–0.4 μm were larger with respect to that associated to the size fraction >10 μm (Fig. 2b, left axis). At a wavelength of 440 nm, the mass specific scattering cross sections for PIM were substantially higher ($1.060 \pm 0.206 \text{ m}^2 \text{ g}^{-1}$) than those corresponding to POM ($0.359 \pm 0.123 \text{ m}^2 \text{ g}^{-1}$) (Fig. 2b, right axis).

In general, the magnitude of the mass normalized absorption coefficient at 440 nm and computed for different size and chemical fractions was higher in UE SF with respect to LE locations (Fig. 3a). Notice that absorption or scattering cross sections for chemical SPM fractions are not shown in UE locations given the insufficient number of samples to perform a multiple regression analysis. In Saguenay Fjord waters, the maximum a_{SPM}^* (440) values (up to $4.6 \text{ m}^2 \text{ g}^{-1}$) were associated with the largest size fraction of SPM (Fig. 3, left axis). Unlike size fractions, no substantial sub regional differences were detected for $\sigma_{\text{a}}^{\text{PIM}}(440)$ and $\sigma_{\text{a}}^{\text{POM}}(440)$ values ($P > 0.05$, t up to 0.42, Student t test) (Fig. 3, right axis). In general, γ and $F_{\text{SPM}}^{\text{PIM}}$ correlations with mass normalized IOPs suggest that particle chemical composition has a larger influence on a_{i}^* (440) (p_s up to 0.50, t up to 12.12, Student t test) with respect to particle size (p_s up to 0.32, t up to 6.85, Student t test) (Table 4). Unlike mass specific absorption coefficients calculated at a wavelength of 440 nm, mass specific scattering coefficients computed at 550 nm and for different size and chemical fractions of SPM presented smaller variations among spatial domains (Fig. 3b). Only for the intermediate size fraction 0.7–10 μm , the regional average of $b_{\text{i}}^*(550)$ in UE SF ($0.432 \pm 0.501 \text{ m}^2 \text{ g}^{-1}$) was larger with respect to that computed in LE waters ($0.136 \pm 0.027 \text{ m}^2 \text{ g}^{-1}$) (Fig. 3b, left axis). Unlike $a_{\text{i}}^*(440)$, $b_{\text{i}}^*(550)$ variability was less influenced by changes on particle composition (p_s up to 0.42, t up to 9.72, Student t test) (Table 4). Conversely, the impact of changing particle dimensions, as inferred from p_s correlations, was greater for $b_{\text{i}}^*(550)$ (p_s up to 0.37, t up to 8.36 Student t test) with respect to $a_{\text{i}}^*(440)$ (p_s up to 0.33, t up to 7.34 Student t test) values. For the spectral interval 400–650 nm, the magnitude of regionally-averaged mass-specific absorption coefficient for unfractionated samples of SPM was higher in SF (e.g., for at $\lambda = 440$ nm, arithmetic average \pm standard error = $0.523 \pm 0.102 \text{ m}^2 \text{ g}^{-1}$) with respect to UE ($0.122 \pm 0.068 \text{ m}^2 \text{ g}^{-1}$) and LE ($0.050 \pm 0.010 \text{ m}^2 \text{ g}^{-1}$) locations (Fig. 2a). Conversely, regionally-averaged mass-specific scattering coefficients of unfractionated samples were highly variable within spatial domains even though highest and lowest values tend to be associated with UE ($0.499 \pm 0.278 \text{ m}^2 \text{ g}^{-1}$) and LE ($0.129 \pm 0.046 \text{ m}^2 \text{ g}^{-1}$) locations, respectively (Fig. 2b). Size-fractioned mass-specific absorption coefficients tended to be higher in SF (e.g., at $\lambda = 440$ nm, up to $2.806 \text{ m}^2 \text{ g}^{-1}$) with respect to other locations of the SLE (up to $2.111 \text{ m}^2 \text{ g}^{-1}$) but for the smallest size range 0.2–0.4 μm where some locations belonging to UE (e.g., st 14) showed higher absorption efficiencies per unit of mass ($2.187 \text{ m}^2 \text{ g}^{-1}$) (Fig. 3a). Spectral curves with the highest a_{i}^* values (e.g., up to 4 m^{-1} at $\lambda = 400$ nm) corresponded with the smallest-sized and largest-sized fractions of SPM (Fig. 3a,d). These values were up to 8 and 5 times higher than those characteristic of

size fractions 0.4-0.7 μm and 0.7-10 μm , respectively (Fig. 3b-c). Similar to a_i^* , highest b_i^* values (up to $5.7 \text{ m}^2 \text{ g}^{-1}$ for $\lambda = 400 \text{ nm}$) corresponded with size fractions having particles with the smallest and the largest diameter (Fig. 4). In general, the spectral slope of b_i^* was very variable in all size fractions (-6 10^{-5} to $6.28 \text{ } 10^{-3} \text{ nm}^{-1}$) with the greatest spectral changes associated to particulates greater than 10 μm . Highest scattering efficiencies in terms of b_i^* were not always measured in the same region. Indeed, maximum b_i^* values for size fraction 0.7-10 μm (up to $1.246 \text{ m}^2 \text{ g}^{-1}$ at $\lambda = 556 \text{ nm}$) and >10 μm (up to $4.579 \text{ m}^2 \text{ g}^{-1}$) were obtained in UE and LE domains, respectively. A common finding was the larger magnitude of size-fractionated mass-specific particulate absorption and scattering coefficients with respect to true optical cross sections of chemical fractions (up to 2 and 3 orders of magnitude for total absorption and scattering, respectively) (Fig. 5). To exemplify these differences, the range of $a_{0.2-0.4 \mu\text{m}}^*$, $a_{>10 \mu\text{m}}^*$, σ_b^{PIM} and σ_b^{POM} values measured at a wavelength of 440 nm and over the whole study area was 0.05 - 2.14 , 0.18 - 1.20 , 0.01 - 1.06 and 0.01 - $1.03 \text{ m}^2 \text{ g}^{-1}$, respectively (Fig. 5a). Likewise, for a wavelength of 556 nm, the range of $b_{0.2-0.4 \mu\text{m}}^*$, $b_{>10 \mu\text{m}}^*$, σ_b^{PIM} and σ_b^{POM} values was 1.82 - 2.39 , 1.05 - 1.49 , 0.08 - 0.36 and 0.07 - $0.38 \text{ m}^2 \text{ g}^{-1}$, respectively (Fig. 5b). In general for the spectral range of 440-556 nm, empirical mass-specific absorption coefficients tended to be higher for particulates within the lower size range (i.e., 0.2-0.4 μm) (Fig. 5a, left-axis). Also, this trend appeared to be reversed at longer wavelengths. Unlike mass-specific absorption coefficients of size fractions, true optical cross sections of chemical fractions showed only differences within the red and near-IR wavelengths (Fig. 5a, right-axis). For the whole study area, the arithmetic average of mass-specific scattering coefficients for the size fraction 0.2-0.4 μm were larger with respect to that associated to the size fraction >10 μm (Fig. 5b, left-axis). At a wavelength of 440 nm, the true scattering cross sections for PIM were substantially higher ($1.060 \pm 0.206 \text{ m}^2 \text{ g}^{-1}$) than those corresponding to POM ($0.359 \pm 0.123 \text{ m}^2 \text{ g}^{-1}$) (Fig. 5b, right-axis). The spatial variation of mass-specific coefficients and true optical cross sections of different fractions of SPM are depicted in Fig. 6. Notice that true absorption or scattering cross sections for chemical fractions of SPM are not shown in UE locations given the insufficient number of samples to perform a multiple regression analysis. In Saguenay Fjord waters, the maximum $a_{\text{SPM}}^*(440)$ values (up to $4.6 \text{ m}^2 \text{ g}^{-1}$) were associated with the size fraction of SPM having particulates greater than 10 μm (Fig. 6a, left-axis). Unlike mass-specific absorption coefficients of SPM size fractions, no substantial sub-regional differences were detected for $\sigma_a^{\text{PIM}}(440)$ and $\sigma_a^{\text{POM}}(440)$ values ($P > 0.05$, t up to 11.5, Student-t test) (Fig. 6a, right-axis). In general, ξ and $F_{\text{SPM}}^{\text{PIM}}$ correlations with size-fractionated mass-specific optical coefficients suggest that particle chemical composition has a larger influence on $a_i^*(440)$ (ρ_s up to 0.50, $P = 0.0009$) with respect to particle size (ρ_s up to 0.32, $P = 0.0033$) (Table 2). The regional average of $b_i^*(550)$ in UE-SF (0.432 - $0.501 \text{ m}^2 \text{ g}^{-1}$) was larger with respect to that computed in LE waters ($0.136 \pm 0.027 \text{ m}^2 \text{ g}^{-1}$) only for particulates within the size range 0.7-10 μm (Fig. 6b, left-axis). Also for SPM fraction having the largest particulates (i.e., > 10 μm), UE locations had typically larger $b_i^*(550)$ values with respect to SF-LE regions. In general and unlike b_i^* , no clear sub-regional differences were observed between $\sigma_b^{\text{PIM}}(440)$ and $\sigma_b^{\text{POM}}(440)$ values ($P > 0.05$, t up to 13.2, Student-t test) (Fig. 6b, right-axis). Unlike $a_i^*(440)$, $b_i^*(550)$ variability was less influenced by changes on particle composition (ρ_s up to 0.42, $P = 0.0015$) (Table 2).

Conversely, the impact of changing particle dimensions, as inferred from ρ_s correlations, was greater for $b_i^*(550)$ (ρ_s up to 0.37, $P = 0.006$) with respect to $a_i^*(440)$ (ρ_s up to 0.32, $P = 0.009$) values.

3.4 Optical proxies

Correlations between individual samples of size-based fractions of SPM and optical proxies of particle size and chemical composition are presented in Table 5. In general, it was found that BOI^{size1} was a more selective biogeo-optical indicator for retrieving second order properties of SPM than BOI^{size2} and BOI^{comp} . Indeed, BOI^{size2} was also dependent on particle chemical composition variations as inferred from F_{SPM}^{PIM} ($\rho_s = -0.16$, $P < 0.05$, $t = 3.40$, Student t test). Likewise, BOI^{comp} changes were also connected to variations of $F_{SPM}^{0.2-0.4 \mu m}$ ($\rho_s = -0.34$, $t = 7.59$, Student t test) and $F_{SPM}^{>10 \mu m}$ ($\rho_s = -0.26$, $t = 5.65$, Student t test) fractions. Despite these dependencies, BOI^{comp} had the strongest correlations with F_{SPM}^{PIM} values ($\rho_s = 0.38$, $P < 0.05$, $t = 8.63$, Student t test). Optical proxies for estimating changes on particle size distributions had a different performance depending on the size fraction. Indeed, Carder et al. (2004) and D'Sa et al. (2007) indices were preferentially associated to changes of relatively small sized (i.e., $F_{SPM}^{0.2-0.4 \mu m}$, ρ_s up to -0.29, t up to -6.36, Student t test) and intermediate sized ($F_{SPM}^{0.4-0.7 \mu m}$, ρ_s up to -0.35, t up to -7.85, Student t test) particulates, respectively (Table 5). Unlike BOI^{comp} , BOI^{size1} and BOI^{size2} indices had a greater correlation with mass specific IOPs and this dependency was stronger for larger particulates and mass normalized absorption coefficients (ρ_s up to 0.74, t up to 23.10 Student t test). Since only three optical cross sections of SPM chemical fractions were computed over the whole study area, correlations between σ_a^i , σ_b^i , BOI^{size1} , BOI^{size2} and BOI^{comp} are not shown. Over the whole study area, there was not a clear relationship between γ and chemical fractions of SPM fractions ($\rho_s = -0.34$, $P = 0.11$). However, γ responded to variations on size fractions for the range 0.2-10 μm (ρ_s up to 0.53, $P = 0.01$). The sign of the relationship changed depending on the size class under investigation (positive for small-sized, negative for intermediate-sized particulates). Although positively correlated, there was not a clear relationship between γ and ξ determinations ($\rho_s = 0.15$, $P = 0.49$, $N = 23$). The range of γ values was 0.759-3.282, 1.389-1.534, 2.873-3.282 and 0.759-1.802 nm^{-1} for the SLE, UE, SF and UE domains. The uncertainty of γ determinations varied between 2.2% and 6.4% with largest errors for samples obtained in LE waters. The spectra slope of a_{SPM}^* was not substantially affected by F_{SPM}^{PIM} changes ($\rho_s = -0.15$, $P = 0.49$, $N = 23$), however $Svis$ variability was strongly influenced by particle size changes within the interval 0.2-0.7 μm ($\rho_s = -0.49$, $P = 0.008$). Range of $Svis$ values of unfractionated samples was 0.005-0.051, 0.009-0.017, 0.014-0.051 and 0.005-0.016 nm^{-1} for the SLE, UE, SF and UE domains, respectively. The uncertainty of $Svis$ estimates varied between 0.5 and 21.5% with largest errors corresponding with samples obtained in LE locations. Over the whole study area, the range of $Svis$ values was 0.004-0.026, 0.007-0.052, 0.004-0.109 and 0.001-0.028 nm^{-1} for size fractions 0.2-0.4 μm , 0.4-0.7 μm , 0.7-10 μm and $> 10 \mu m$, respectively. In general, $Svis$ slopes were not correlated between size fractions even though the magnitude of $Svis$ for total unfractionated samples was strongly influenced by $Svis$ calculated for the 0.7-10 μm fraction ($\rho_s = 0.66$, $P = 0.004$).

4 Discussion

4.1 Uncertainty of optical properties coefficients

Inherent optical properties in this study were derived from an ac-s instrument. Thus, large errors on absorption coefficients may be anticipated in relatively turbid waters if original measurements are not corrected by scattering effects (Boss et al., 2009; McKee et al., 2013). These effects are mainly attributed the acceptance angle of the transmissometer and the multiple scattering of photons. The acceptance angle of the ac-s instrument is $\sim 0.9^\circ$ and much larger than that corresponding to the LISST-100X diffractometer ($\sim 0.027^\circ$). Thus, a larger underestimation on c magnitude is expected in ac-s with respect to LISST-100X measurements due to a larger contribution of forward-scattered photons arriving to the detector of the former optical instrument. Further comparisons of $c(532)$ measurements derived here by ac-s and LISST-100X showed that c values as derived from ac-s were 23-84% lower with respect to those determinations based on LISST-100X. This is consistent with Boss et al. (2009) who reported that uncorrected Wet Labs ac-9 attenuation values are approximately 50%-80% of equivalent LISST attenuation data. Unfortunately, c deviations due to acceptance angle variations were not corrected in this study due to the lack of true c values as obtained by using an integrating cavity absorption meter (e.g., PSICAM) (Röttgers et al., 2005). Notice that these errors are much greater with respect to the optical variability associated to each sample determination as computed from ac-s measurements (e.g., $< 1\%$ at $\lambda = 532$ nm).

In this investigation, the ‘flat’ baseline correction was selected for correcting residual scattering in absorption coefficient estimates as derived from ac-s measurements. This technique was chosen due to the lack of PSICAM measurements or critical ancillary optical information (e.g., particle backscattering efficiency) to tune up a Monte Carlo scattering correction approach (McKee et al., 2008). The ‘flat’ scattering correction approach is expected to provide a fair correction of a values in oceanic waters (up to 15% underestimation at wavelengths shorter than 600 nm, see Fig. 8b, McKee et al., 2013) but may result in large deviations (up to 100% decrease in the NIR) of a values in relatively turbid waters (e.g., $a > 0.2 \text{ m}^{-1}$) such as the Baltic/North Sea. Also, this issue is present when the proportional correction method of Zaneveld et al. (1994) is applied. Unlike the ‘flat’ baseline, the scattering residual of the proportional method is spectrally dependent but still relying in one reference wavelength in the NIR spectral range. Approximations justifying the use of the ‘flat’ (i.e., zero absorption signal in the NIR) and ‘proportional’ (i.e., wavelength-dependent scattering phase function) method are still in debate (McKee et al., 2013). Lastly, the Monte Carlo correction method (McKee et al., 2008) has in general better agreement (error $< 10\%$) with true a values as derived from an integrating cavity absorption meter. However, this approach may also have major uncertainties due to assumptions regarding optical coefficients^{IOPs} (e.g., particulate backscattering ratio and volume scattering function) and changes on scattering efficiency by the inner wall of the reflective tube due to aging (McKee et al., 2013). Thus in conclusion, the resulting particle-related IOPs and mass-specific optical coefficients obtained in the SLE-SF waters may present large errors (i.e., $> 50\%$) with respect to true values and at wavelengths longer than 550 nm. This bias is anticipated to be maximum (minimum) in UE (LE) locations.

4.2 Spatial patterns of SPM microphysical characteristics Variability of microphysical properties of SPM

A striking finding in this study was the important weight contribution of relatively large particulates (i.e., $>10 \mu\text{m}$) in UE waters. This phenomenon was likely attributed to the active resuspension of sediments associated with vertical mixing produced by tidal currents and winds (Yeats, 1988). Conversely, this effect was secondary in relatively deep waters of SF and LE where large and heavy particulates are rapidly removed from the water column and deposited along submarine canyons (Gagné et al., 2009).

Although chemical composition of SPM size fractions was not analyzed in this study, additional correlations between total $F_{\text{SPM}}^{\text{PIM}}$ and SPM size fractions values suggest that suggest that particulates smaller than $10 \mu\text{m}$ were richer in inorganic matter ($\rho_s = 0.62$, $P < 0.001$, $N = 23$) with respect to particulates with a diameter greater than $10 \mu\text{m}$ smallest particulates were richer in inorganic matter ($\rho_s = -0.27$, t up to 5.89 , Student-t test, Table A2). Also, the opposite was true for the largest particulates ($\rho_s = -0.27$, t up to -5.89 , Student-t test). This finding confirms previous studies showing that relatively small ($\sim 2 \mu\text{m}$) particulates in the SLE are mainly composed by minerals (Yeats, 1988; Gagné et al., 2009).

In this contribution, a large proportion of particulates with a diameter above $50 \mu\text{m}$ and lower γ values were typically found in LE locations. This regional variation in SPM size distribution was attributed to the major influence of large sized particulates derived from phytoplankton as γ was strongly correlated with chlorophyll a concentration ($\rho_s = 0.45$, t up to 10.58 , Student-t test, Table A3). In this contribution, a large proportion of particulates with a diameter above $50 \mu\text{m}$ and lower ξ values were typically found in LE locations. These results also support historical observations made during July and August and showing a greater proportion of relatively large particulates (i.e., > 5 and $< 50 \mu\text{m}$) over the LE locations (Chanut and Poulet, 1979).

20 4.3 Spatial variability of mass-specific optical coefficients

In this study, a_{SPM}^* measurements in the visible and near-IR range were in the upper range or higher than those reported in the literature for temperate coastal waters (e.g., Mobile Bay, River of La Plata, Elbe Estuary, Gironde Estuary) (Stavn and Richter, 2008; Doxaran et al., 2009; Dogliotti et al., 2015) (Table 64). In general, lowest a_{SPM}^* values commonly corresponded with samples obtained in very turbid environments (i.e., $> 100 \text{ g m}^{-3}$, Gironde River, La Plata River) (Dogliotti et al., 2015; Doxaran et al., 2009). Notice that part of this decrease can be attributed to an incomplete removal of multiple scattering effects. Relative low a_{SPM}^* values have been linked to high POC/SPM (Wozniak et al., 2010) and chl/SPM concentration ratios, where chl means chlorophyll a (Estapa et al., 2012). In this study, chl/SPM presented values as high as $2 \cdot 10^{-3}$ that are comparable to relatively high ratios reported by D'Sa et al. (2006). Thus, it is suggested that some locations in our study area are characterized by relatively high POC/SPM as other turbid coastal environments such as adjacent waters to the Mississippi Delta (D'Sa et al. 2006).

One mechanism explaining the general decrease of a_{SPM}^* in very turbid waters is related to packaging effects (Morel, 1974; Zhang et al., 2014). At higher turbidities, particulates become dominated by larger size distributions, thus as mean diameter

of particles increases, the scattering efficiency of SPM decreases. In SF waters, the magnitude of $a_{>10\text{ }\mu\text{m}}^*(440)$ values were higher with respect to those computed in other SLE sub regions. A well-known mechanism explaining the general decrease of a_{SPM}^* in very turbid waters is related to packaging effects (Morel, 1974; Zhang et al., 2014). At higher turbidities, larger particulates contribute to PSD variations, thus as mean diameter of particles increases, the light absorption efficiency per averaged particle decreases (i.e., the interior of larger particles has a greater 'shading'). These differences could be related to the relatively high concentrations of particulate iron in surface waters of the Saguenay Fjord (Yeats and Bewers, 1976; Tremblay and Gagné, 2009). Pigmentation of mineral particulate due to iron hydroxides has been suggested to be a major factor enhancing a_{SPM}^* (Babin and Stramski, 2004; Estapa et al., 2012). This could also explain the spatial differences of $a_{\text{SPM}}^*(440)$ in our study area where larger values corresponded with surface waters dominated by particles assemblages having a smaller mean diameter (i.e., UE and SF). In nearshore waters of California, Wozniak et al. (2010) demonstrated inverse relationships between $a_{\text{SPM}}^*(440)$ and the median particle diameter for inorganic- and organic-dominated assemblages. Also and consistent with our previous discussion regarding particle composition, Wozniak et al. (2010) observed that POC/SPM was positively correlated with the median particle diameter. Indirect size effects on $a_{\text{SPM}}^*(440)$ due to changes on iron content per particle have been discussed by Estapa et al. (2012). In general, smaller particulates have a greater surface for adsorbing organic compounds where iron can accumulate (Mayer, 1994; Poulton and Raiswell, 2005). Thus, SPM fractions with smaller particulates are expected to have an enhancement of $a_{\text{SPM}}^*(440)$ due to high iron concentrations. This phenomenon likely explained our higher $a_{\text{SPM}}^*(440)$ in SF regions with respect to LE waters where the water salinity range is 0-29 and 29-33.5, respectively (El Sabh, 1988). Indeed, relatively high concentrations of particulate iron have been measured in surface waters of the Saguenay Fjord (Yeats and Bewers, 1976; Tremblay and Gagné, 2009). In coastal Louisiana and the lower Mississippi and Atchafalaya rivers, Estapa et al. (2012) found that magnitude of a_{SPM}^* within the UV ($\lambda \sim 360\text{-}390\text{ nm}$) and blue ($\lambda \sim 400\text{-}450\text{ nm}$) spectral range is commonly higher in freshwater with respect to marine samples. This is related to the greater concentration of particulate iron oxides and hydroxides derived from terrestrial sources in freshwater samples and later transport and reduction in marine environments. Iron oxide and hydroxide minerals have a major light absorption within the spectral range of 400-450 nm due to the absorption bands of iron (Estepa et al., 2012). Pigmentation of mineral particulates due to iron hydroxides has been suggested to be a major factor increasing a_{SPM}^* (Babin and Stramski, 2004; Estapa et al., 2012). Unfortunately and unlike optical measurements made by Estapa et al. (2012), the resolution of our ac-s measurements (~4 nm) did not allow a deeper analysis of iron absorption peaks by performing a second-derivative calculation. In general, σ_n^{POM} and σ_n^{PIM} values were within the range of values reported in the literature with the exception of SF locations where mass-specific absorption cross sections were substantially higher (up to 1.71 and 0.86 $\text{m}^2\text{ g}^{-1}$, respectively, $\lambda = 440\text{ nm}$). This difference was likely attributed to the aforementioned enhancement of light absorption due to particulate iron-enrichment in SF waters.

Unlike a_{SPM}^* , the magnitude of b_{SPM}^* during our surveys was comparable, smaller or higher with respect to other studies depending on the wavelength and the type of environment. To exemplify, at the wavelength of 440 nm, the magnitude of our b_{SPM}^* measurements was comparable to that reported in coastal waters off Mississippi (Stavn and Richter, 2008). However, these values were higher compared to that reported in the Irish Sea waters (Bowers and Binding, 2006). The magnitude of σ_b^{POM} in our study area was relatively low with respect to those values reported in other littoral environments (e.g., Monterrey Bay, Mobile Bay and off New Jersey shore) (Snyder et al., 2008; Zhang et al., 2014).

Similar to a_{SPM}^* , b_{SPM}^* values were highly variable between locations and within the range of measurements obtained in other environments (Table 4). In this study, the spectral variation b_{SPM}^* between regions showed a spectral flattening as particle assemblages become dominated by organic matter (i.e., LE). This finding is consistent with Wozniak et al. (2010) measurements made in Imperial Beach, California. Our measurements of scattering cross sections of PIM in the SLE were higher with respect to other littoral regions of the world. For instances, $\sigma_b^{PIM}(440)$ in the SLE was up to 2-fold the magnitude of maximum $\sigma_b^{PIM}(440)$ values measured in off New Jersey coast by Snyder et al. (2008). The origin of these differences is unknown and could be mainly related to mineral composition variations and associated iron as particle size distribution measurements during our surveys were comparable to those published by other studies. Unlike σ_b^{PIM} , our σ_b^{POM} estimates were within the range of values obtained in the Gulf of Mexico and along the east coast of US.

4.4 Particle size and composition effects on mass-specific optical coefficients

Correlations of γ and F_{SPM}^{PIM} with mass normalized IOPs for different SPM size fractions showed two contrasting optical responses (Table 4). Correlations of ξ and F_{SPM}^{PIM} with mass-specific optical coefficients for different SPM size fractions were shown in Table 2. First, γ was positively correlated with $a_i^*(440)$ (ρ_s up to 0.31, t up to 7.34, Student t test) and $b_i^*(550)$ (ρ_s up to 0.37, t up to 14.19, Student t test) for particulates larger than 10 μm . This pattern was due probably to the greater changes in particle density and associated variations on optical properties per unit of mass as particulates get bigger and more hydrated (Neukermans et al., 2012; Neukermans et al 2016; Reynolds et al., 2016). This effect is mainly observed in undisrupted marine aggregates (Slade et al. 2011). Since particle aggregates were altered during our experiments, this process is expected to be less important in explaining optical changes of suspended particulates. Based on theoretical calculations, Babin et al. (2003) showed a positive relationship between $b_{SPM}^*(550)$ and the differential Junge slope of particle size distribution. Also in this study, $b_{SPM}^*(550)$ was found to be directly related to γ (Table 4). For all size fractions, ξ was positively correlated with $a_i^*(440)$ (ρ_s up to 0.32, $P = 0.006$). This pattern is consistent with the higher absorption efficiency of relatively small-sized particulates. As previously discussed, these particulates have a greater light absorption per unit of particle mass due to iron-enrichment and a lesser role of shading effects. Since particle aggregates were altered during our experiments, the influence of particle density on mass-specific optical coefficients cannot be quantified as this effect is mainly observed in undisrupted marine aggregates (Slade et al. 2011; Neukermans et al., 2012; Neukermans et al.

2016). However and based on Estapa et al. (2012) simulations, the impact of aggregation on a_{SPM}^* is anticipated to be small (i.e., ~10%) with respect to the spatial variability of a_{SPM}^* in SLE-SF waters.

In general, ξ was positively correlated with $b_i^*(550)$ (ρ_s up to 0.37, $P = 0.008$) and pointed out as expected the higher scattering efficiency of small-sized particulates due to the smaller influence of packaging effects. Notice that ξ correlations with $b_i^*(550)$ were greater with respect to $a_i^*(440)$ and more remarkable for relatively large-sized particulates. In Arctic waters, Reynolds et al. (2016) observed an increase on mass-specific particulate backscattering for mineral-rich particle assemblages that tend to exhibit steeper size distributions. Although no particulate backscattering measurements were available in this study, Reynolds et al. (2016) highlight the importance of relatively small-sized particulates for driving variations on mass-specific optical coefficients linked to scattering processes.

5

10

15

20

25

30

F_{SPM}^{PIM} had a stronger correlation with $a_i^*(440)$ compared with $b_i^*(550)$ values, and these relationships were stronger when SPM was dominated by particulates with an intermediate size (i.e., 0.4-10 μm). Babin et al. (2004) obtained positive correlations between a_{SPM}^* and iron content of minerals. In Arctic waters, Reynolds et al. (2016) observed an increase on mass specific particulate backscattering for mineral rich particle assemblages that tend to exhibit steeper size distributions. In summary, our results indicate that size (chemical composition) of suspended particulates has a major influence on spatial variability of b_i^* (a_i^*) in SLE-SF waters.

In all cases, F_{SPM}^{PIM} had a stronger correlation with $a_i^*(440)$ compared with $b_i^*(550)$ values, and these relationships were stronger when SPM was dominated by particulates with an intermediate size (i.e., 0.4-10 μm). The enrichment of suspended particulates on inorganic matter and concomitant variations $a_i^*(440)$ may be explained by a greater contribution of mineral-associated iron to light absorption. Also, the combustion method used to measure PIM in our study could be another factor explaining the increased particle absorption in the blue range (Babin et al. 2003). Iron can take many forms in mineral particulates (oxides, hydroxides, monosulfides) and can be deposited over the particle surface or be part of its internal structure (e.g., clays). Since the mean diameter of clay particles is less than 2 μm , the aforementioned F_{SPM}^{PIM} - $a_i^*(440)$ correlations were also likely affected by iron associated (adsorbed or structural) to other types of inorganic particulates that are characterized by larger dimensions. In SF locations, reduced iron is mainly associated to dissolved organic compounds that can be strongly adsorbed to hydrous metal oxides (Deflandre et al., 2002). Babin and Stramski (2004) obtained positive correlations between a_{SPM}^* and iron content of dust and soil particles suspended in seawater. Estapa et al. (2012) found a strong covariation between a_{SPM}^* values and dithionite-extractable iron content of oxides and hydroxides.

An important objection to correlations of ξ and F_{SPM}^{PIM} with mass-specific optical coefficients of SPM size fractions was related to differences in terms of particle size range used to compute ξ and F_{SPM}^{PIM} and particle size classes derived by sequential filtration of water samples. More specifically, ξ is not representative of submicron particles less than 2 μm . Also, F_{SPM}^{PIM} is only a valid particle composition parameter for particles mostly larger than 0.7 μm . Thus, correlations ξ and F_{SPM}^{PIM} with mass-specific optical coefficients of 0.2-0.4 μm and 0.4-0.7 μm may only reflect indirect dependencies between

mass-normalized optical coefficients of different size classes. This possibility (i.e., correlations between a_i^* or b_i^* of different size classes) was confirmed based on samples obtained in UE, LE and SF waters. Lastly, it is important to discuss the potential bias on a_i^* and b_i^* determinations due to size fractionation and *a posteriori* impact on correlations with respect to F_{SPM}^{PIM} and ξ . No measurements of F_{SPM}^{PIM} and ξ were done in size fractions of SPM, thus it is difficult to compare particulate size distribution and chemical composition changes before and after the size fractionation of the samples. Size fractionation is anticipated to cause retention of smaller particulates in membranes having a larger pore size. These primary particles will overestimate the weight of the filtered sample and underestimate the weight of the next filtration step consisting in a membrane having a smaller pore size. Since particle sieving begins with large-sized particles and finishes with small-sized particles, the magnitude of a_i^* and b_i^* for relatively large (small) particulates is likely to be under-(over-)estimated. Bias on mass of size fractions was verified by comparing the sum of masses for 0.7-10 μm and >10 μm with the total sample filtered through a GF/F filter (i.e., 0.7 μm nominal pore size). The arithmetic average of relative bias for the whole study area was 31.4% or a 31.4% overestimation of mass for particulates > 0.7 μm when total weight is computed based on sum of partial weights corresponding to different size fractions. An optimization scheme to adjust the mass for each size fractions (i.e. adjusting the various masses to sum up to the total mass filtered) was not attempted since we didn't filter total samples through 0.2 or 0.4 μm membranes due to the sequential mode of our filtration. Thus, 'filtration weighting factors' for size fractions > 0.2 μm or > 0.4 μm could not be calculated.

4.5 Optical proxies of particle size and composition characteristics

The response of three optical composite variables (BOI^{size1} , BOI^{size2} and BOI^{comp}) to changes on size and composition of different particle assemblages was evaluated based on correlation analysis. In general, BOI^{size1} was the most selective optical index for tracking variations on particle micro physical properties. Indeed, BOI^{comp} (BOI^{size2}) was also substantially affected by size distribution (chemical composition) of SPM. The lack of specificity of BOI^{comp} may respond to the use of a spectral range where phytoplankton has a maximum light absorption peak (i.e., $\lambda = 675 \text{ nm}$). As phytoplankton cells become larger (e.g., above 20 μm), the total chlorophyll a concentration of phytoplankton cells increases (Montes Hugo et al., 2008). As a result, the magnitude of a_{SPM} at a wavelength of 675 nm is expected to increase affecting positively BOI^{comp} . Lastly, BOI^{size1} and BOI^{size2} response was mainly associated with variability of small sized and intermediate sized SPM fractions, respectively. This selectivity is particularly interesting as both indexes may be combined for developing more robust metrics for estimating SPM size spectra distributions in littoral waters.

In terms of fractioned mass, the size of particulates was the dominant variable driving changes on γ (ρ_s up to 0.53, $P = 0.004$). Conversely, the mineral content of SPM did not have a statistically detectable impact at 95% confidence interval. In particular, the strongest response of γ to size effects was manifested for the mass fraction having the smallest particulates (i.e., 0.2-0.4 μm). Despite the major effects of particle size classes on γ , values of γ were not clearly correlated with ξ slopes. In oceanic waters, ξ and γ values are expected to covary in a linear way for a specific range of refractive index and ξ (Boss et

al., 2001; Twardowski et al., 2001). Our range of ξ values was within the natural variability reported in coastal and oceanic environments ($\xi = 2-4.5$) (Reynolds et al., 2010; Neukermans et al., 2012; Xi et al., 2014). Also, the magnitude of γ in our samples ($0.29-2.22 \text{ nm}^{-1}$) was within the range of values that characterize oceanic environments (0.2-2) (Twardowski et al., 2001, Boss et al., 2013). Unlike oceanic waters, the poor correspondence between ξ and γ values in this study was linked to different responses of spectral c_{SPM} and particle size distribution slopes to changes of two non-covarying optical contributions: minerals and phytoplankton. Also, the reduced number of sampling locations and the geographic variability of ξ - γ relationships were additional factors likely explaining the lack of a general functionality for the study area. Lastly, ξ and γ were not substantially correlated in our samples due to deviations on Mie-based models (e.g. absorbing spheres) of γ as a function of ξ (Twardowski et al., 2001). Indeed during our surveys, high absorbing particulates were present in SLE-SF waters.

The variability of S_{vis} values in this study was relatively high (~10-fold) with respect to other littoral environments (1.3-fold, $S_{\text{vis}} = 0.009-0.0113 \text{ nm}^{-1}$) (Estapa et al., 2012). Since S_{vis} was preferentially influenced in a direct way by the contribution of small-sized particulates within the range 0.2-0.4 μm , it is feasible a potential link between S_{vis} and particulate iron of small-sized mineral particulates (Estapa et al., 2012). No statistically significant correlations at 95% confidence level were computed between $F_{\text{SPM}}^{\text{PIM}}$ and S_{vis} . This is counterintuitive as $F_{\text{SPM}}^{\text{PIM}}$ is positively related to a_{SPM}^* and presumably iron content of particulates. This discrepancy might be related to the inclusion of freshwater or brackish samples into the correlation analysis as S_{vis} is only expected to change with extractable-iron of marine measurements (Estapa et al., 2012). More specific correlations by only using LE measurements supported this hypothesis ($\rho_{\text{LE}} = 0.58$, $P = 0.023$). Thus, our results suggest that S_{vis} is likely an indicator of iron associated to mineral-enriched particulates in LE waters.

20 5 Conclusions

The measure of optical cross sections of SPM is essential for developing optical inversions and improve our understanding regarding the origin of optical signatures in remote sensing studies and map biogeo-chemical components in surface waters. In this contribution, we presented for the first time, mass-specific scattering and absorption coefficients of size fractionated SPM in estuarine waters of the Saint Lawrence River and a major SLE tributary, the Saguenay Fjord.

25 Despite the intrinsic variability of weight-normalized IOPs due to variations of particle micro physical attributes, the following trends were observed: 1. the mass-specific absorption coefficient of SPM was preferentially influenced by changes in particle chemical composition, 2. particle size had a larger impact on b_{SPM}^* than a_{SPM}^* , and 3. optical proxies of SPM size distribution BOI^{size} was more specific than optical proxy related to particle chemical composition (i.e., BOI^{comp}). These relationships are anticipated to be useful in the context of predicting mass-specific IOPs based on satellite remote sensing measurements. optical coefficients due to variations of particle micro-physical attributes, the following patterns were identified: 1. the mass-specific absorption coefficient of SPM was preferentially influenced by changes in particle chemical composition as inferred from changes on $F_{\text{SPM}}^{\text{PIM}}$, 2. regional variations on S_{vis} suggest a substantial iron-enrichment of

5 suspended particulates in LE waters, 3. a_{SPM}^* (440) values were usually higher in SF-UE with respect to LE locations for all size fractions and indicate that iron is not selectively bounded to specific size class of particulates, 4. $Svis\text{-}F_{SPM}^{PIM}$ correlations in LE locations suggest a potential iron-enrichment of particulates having a larger mineral content, 5. salinity was an important variable correlated with changes on a_{SPM}^* at the regional scale, 6. size spectra of particulates had a larger impact on b_{SPM}^* than a_{SPM}^* , and 7. no clear regional differences were established in terms of b_{SPM}^* magnitude or spectral variation. In summary, the aforementioned relationships will be useful in investigating local and regionally-limited relationships and properties of SPM.

6 Funding

10 This investigation was supported by the Natural Sciences and Engineering Research Council of Canada, Individual Discovery grant, project title: "Optical remote Sensing models of suspended Particulate matter in the St. Lawrence Estuary "(OSPLE), awarded to Dr. Martin Montes Hugo.

7 Acknowledgements

15 We thank to the crew of the Creed and Mr. Alexandre Palardy for their assistance during the field work. Also, we appreciate the support of ISMER technicians Mr. Pascal Rioux and Ms. Dominique Lavallée during the field surveys and the processing of lab measurements.

References

Agrawal, Y., McCave I. and Riley J.: Laser diffraction size analysis, in Principles, Methods, and Application of Particle Size Analysis, edited by James P. M. Syvitski, pp. 119–129, Cambridge University Press, N. Y., 1991.

20 Agrawal, Y. C., A. Whitmire, O. A. Mikkelsen and H. C. Pottsmith H.C.: Light scattering by random shaped particles and consequences of measuring suspended sediments by laser diffraction, *J. Geophys. Res.*, 113, C04023, doi:10.1029/2007JC004403, 2008.

Andrews, S., D. Nover and S. G. Schladow: Using laser diffraction data to obtain accurate particle size distributions: The role of particle composition, *Limnol. Oceanogr.: Methods* 8, 507–526. doi:10.4319/lom.2010.8.507, 2010.

25 Babin, M., Therriault, J.C., Legendre, L. and Condal, A.: Variations in the specific absorption coefficient for natural phytoplankton assemblages: Impact on estimates of primary production, *Limnol. Oceanogr.*, 38, 154-177, 1993.

Babin, M., Stramski D., Ferrari G.M., Claustre H., Bricaud, A., Obolensky, G. and Hoepffner N.: Variations in the light absorption coefficients of phytoplankton, nonalgal particles, and dissolved organic matter in coastal waters around Europe, *J. Geophys. Res.*, 108, 10.1029/2001JC000882, 2003.

Babin, M. and Stramski, D.: Variations in the mass-specific absorption coefficient of mineral particles suspended in water, Limnol. Oceanogr., 49, 756–767, 2004.

Barillé-Boyer, A.L., Barillé, L., Massé, H., Razet, D. and Héral, M: Correction for particulate organic matter as estimated by loss on ignition in estuarine ecosystems, Estuar. Coast. Shelf Sci., 58, 147–153, 2003.

5 Bernatchez, P. and Dubois, J.-M. M.: Bilan des connaissances de la dynamique de l'érosion des côtes du Québec maritime laurentien, Géographie Phys. Quat., 58, 45, 2004 (in french).

Bettioli, C., Stevano, L., Bertelle, M., Delfino, F., and Argese, E.: Evaluation of microwave-assisted acid extraction procedures for the determination of metal content and potential bioavailability in sediments. Appl. Geochem. 23, 1140–1151, 2008.

10 Binding, C.E., Bowers, D.G. and Mitchelson-Jacob, E.G.: Estimating suspended sediment concentrations from ocean colour measurements in moderately turbid waters; the impact of variable particle scattering properties, Rem. Sens. Environ., 94, 373–383, 2005.

15 Boss, E., Twardowski, M.S., and Herring, S.: Shape of the particulate beam attenuation spectrum and its relation to the size distribution of oceanic particles, App. Opt. 40, 4885–4893, 2001.

Boss, E., Slade, H., Behrenfeld, M. and Dall'Olmo, G.: Acceptance angle effects on the beam attenuation in the ocean, Opt. Expr., 17, 1535–1550, 2009.

20 Boss, E., Picheral, M., Leeuwa, T., Chase, A., Karsenti, E., Gorsky, G., Taylor, L., Slade, W., Ras, J., Claustre, H.: The characteristics of particulate absorption, scattering and attenuation coefficients in the surface ocean: Contribution of the Tara Oceans expedition, Methods in oceanography, 7, 52–62, 2013.

Bowers, D. G. and Binding, C. E.: The optical properties of mineral suspended particles: A review and synthesis, Estuar. Coast. Shelf Sci., 67, 219–230, 2006.

25 Bowers, D.G., Braithwaite, K.M., Nimmo-Smith, W. A. M. and Graham, G. W.: Light scattering by particles suspended in the sea: The role of particle size and density, Cont. Shelf Res., 29, 1748–1755, 2009.

Bricaud, A. and Stramski, D.: Spectral absorption coefficients of living phytoplankton and nonalgal biogenous matter: A comparison between Peru upwelling area and the Sargasso Sea, Limnol. Oceanogr., 35, 562–582, 1990.

30 Carder, K. L., Chen, F. R., Cannizzaro, J. P., Campbell, J. W., and Mitchell, B. G.: Performance of the MODIS semi-analytical ocean color algorithm for chlorophyll a, Adv. Sp. Res., 33, 1152–1159, 2004.

Chanut, J. P. and Poulet, S. A.: Short-term variability of the size spectra of suspended particles in a rapidly changing environment., Estuar. Coast. Shelf Sci., 15, 497–513, 1982.

D'Anglejan, B. F. and Smith, E. C.: Distribution, Transport, and Composition of Suspended Matter in the St. Lawrence Estuary, Can. J. Earth Sci., 10, 1380–1396, 1973.

Dalu, T., Richoux, N. B., and Froneman, P. W.: Nature and source of suspended particulate matter and detritus along an austral temperate river-estuary continuum, assessed using stable isotope analysis, *Hydrobiologia*, 767, 95-110, 2016.

Deflandre B., Mucci, A., Gagne, J.P., Guignard, C., Sundby, and B.: Early diagenetic processes in coastal marine sediments disturbed by a catastrophic sedimentation event. *Geochimica et Cosmochimica Acta*, 66, 2547-2558,2002.

5

Devlin, M. J., Barry, J., Mills, D. K., Gowen, R. J., Foden, J., Sivyer, D., and Tett, P.: Relationships between suspended particulate material, light attenuation and Secchi depth in UK marine waters, *Estuar. Coast. Res. Shelf Sci.*, 79, 429-439, 2008.

D'Sa, E. J., Miller, R. L. and McKee, B. A.: Suspended particulate matter dynamics in coastal waters from ocean color: Application to the northern Gulf of Mexico. *Geophys. Res. Lett.*, 34, 1-6, 2007.

Dogliotti, A. I., Ruddick, K. G., Nechad, B., Doxaran, D. and Knaeps, E.: A single algorithm to retrieve turbidity from remotely-sensed data in all coastal and estuarine waters, *Remote Sens. Environ.*, 156, 157-168, 2015.

Doxaran, D., Froidefond, J. M., Lavender, S., and Castaing, P.: Spectral signature of highly turbid waters: Application with SPOT data to quantify suspended particulate matter concentrations, *Remote Sens. Environ.*, 81, 149-161, 2002.

15 Doxaran, D., Ruddick, K., McKee, D., Gentili, B., Tailliez, D., Chami, M. and Babin, M.: Spectral variation of light scattering by marine particles in coastal waters, from visible to near infrared, *Limnol. Oceanogr.*, 54, 1257-1271, , 2009.

D'Sa E.J., Miller R.L., and Del Castillo C: Bio-optical properties and ocean color algorithms for coastal waters influenced by the Mississippi River during a cold front. *Appl. Opt.*, 45,7410-7428, 2006.

El-Sabhy, M.J.: Physical oceanography of the St. Lawrence estuary. In: Kjerfve, B. (Ed.), *Hydrodynamics of Estuaries, Estuarine Case Studies*, vol. II. CRC Press, Boca Raton, Florida, pp. 61-78, 1988.

Estapa, M. L., Boss, E., Mayer, L. M. and Roesler, C. S.: Role of iron and organic carbon in mass-specific light absorption by particulate matter from Louisiana coastal waters, *Limnol. Oceanogr.*, 57, 97-112, 2012.

25 Fauchot, J., Saucier, F. J., Levasseur, M., Roy, S. and Zakardjian, B.: Wind-driven river plume dynamics and toxic Alexandrium tamarensis blooms in the St. Lawrence estuary (Canada): A modeling study, *Harmful Algae*, 7, 214-227, 2008.

Gagné, H., Lajeunesse, P., St-Onge, G. and Bolduc, A.: Recent transfer of coastal sediments to the Laurentian Channel, Lower St. Lawrence Estuary (Eastern Canada), through submarine canyon and fan systems, *Geo-Marine Lett.*, 29, 191-200, 2009.

Gordon, H.R., Brown, O.B., Evans, R.H., Brown, J.W., Smith, R.C., Baker, K.S., Clark, D.K., A semi-analytic radiance model of ocean color. *J. Geophys. Res.*, 93, 10909-10924, 1988.

Guinder, V. A., Popovich, C. A., and Perillo, G. M. E.: Particulate suspended matter concentrations in the Bahia Blanca Estuary, Argentina: Implication for the development of phytoplankton blooms, *Estuar. Coast. Res. Shelf Sci.*, 85, 157-165, 2009.

Junge, C. E.: Air chemistry and radioactivity, Acad. Press INC, 11, 1253, , 1963.

Larouche, P. and Boyer-Villemaire, U.: Suspended particulate matter in the St. Lawrence estuary and Gulf surface layer and development of a remote sensing algorithm, *Estuar. Coast. Shelf Sci.*, 90, 241–249, 2010.

Levasseur, M., Therriault, J.-C. and Legendre, L.: Hierarchical control of phytoplankton succession by physical factors, *Mar. Ecol. Prog. Ser.*, 19, 211–222, 1984.

5 Loisel, H., Nicolas, J. M., Sciandra, A., Stramski, D. and Poteau, A.: Spectral dependency of optical backscattering by marine particles from satellite remote sensing of the global ocean, *J. Geophys. Res. Ocean.*, 111, 1–14, 2006.

Loisel, H., Duforet, L., Dessailly, D., Chami, M., and Dubuisson, P.: Investigation of the variations in the water leaving polarized reflectance from the POLDER satellite data over two biogeochemical contrasted oceanic areas, *Opt. Exp.*, 17, 12905–12918, 2008.

10 Löptien, U. and Meier, H. E. M.: The influence of increasing water turbidity on the sea surface temperature in the Baltic Sea: A model sensitivity study, *J. Mar. Syst.*, 88, 323–331, 2011.

Ma, H., Kim, S. D., Allen, H. E., and Cha, D. K.: Effect of copper binding by suspended particulate matter on toxicity, *Environ. Toxicol. Chem.* 21, 710–714, 2002.

15 McKee, D., Piskozub, J. and Brown, I.: Scattering error corrections for in situ absorption and attenuation measurements, *Opt. Exp.*, 16, 19480–19492, 2008.

McKee, D., Piskozub, J., Röttgers, R., Reynolds, R.A.: Evaluation and improvement of an iterative scattering correction scheme for in situ absorption and attenuation measurements, *J. Amer. Ocean. Technol.*, 30, doi.10.1175/JTECH-D-12-00150.1, 2013.

20 Miller, R. L. and McKee, B. A.: Using MODIS Terra 250 m imagery to map concentrations of total suspended matter in coastal waters, *Remote Sens. Environ.*, 93, 259–266, 2004.

Mohammadpour, G., Montes-Hugo, M. A., Stavn, R., Gagné, J. P. and Larouche, P.: Particle Composition Effects on MERIS-Derived SPM: A Case Study in the Saint Lawrence Estuary, *Can. J. Remote Sens.*, 41, 515–524, 2015.

25 Montes Hugo, M., Vernet, M., Martinson, D., Smith, R. and Iannuzzi, R.: Variability on phytoplankton size structure in the western Antarctic Peninsula (1997–2006), *Deep-Sea Res. Part II Top. Stud. Oceanogr.*, 55, 2106–2117, 2008.

Montes-Hugo, M. A. and Mohammadpour, G.: Biogeo-optical modeling of SPM in the St. Lawrence Estuary, *Can. J. Remote Sens.*, 38, 197–209, 2012.

Morel, A.: Optical properties of pure water and pure seawater, p.1–24, In: N.G. Jerlov and E. Steemann Nielsen (eds.), *Optical aspects of oceanography* Academic, 1974.

30 Morel, A. and Antoine, D.: Heating Rate within the Upper Ocean in Relation to its Bio-optical State, *J. Phys. Oceanogr.*, 24, 1652–1665, 1994.

Morel, A. and Prieur, L.: Analysis of variations in ocean color, *Limnol. Oceanogr.*, 22, 709–722, 1977.

Morel, A. and Gentili, B.: Diffuse reflectance of oceanic waters. III. Implication of bidirectionality for the remote sensing problem., *Appl. Opt.*, 35, 4850–4862, 1996.

Müller HW. and Horn K., Some Technical Aspects of a High Quality UV/Vis Spectrometer for Routine Analysis, Applied UV Spectroscopy 19D, Bodenseewerk Perkin Elmer GmbH, Überlingen, 1990.

Neukermans, G., Loisel, H., Mériaux, X., Astoreca, R. and McKee, D.: In situ variability of mass-specific beam attenuation and backscattering of marine particles with respect to particle size, density, and composition, Limnol. Oceanogr., 57, 124–144, 2012.

Neukermans, G., Reynolds, R. A. and Stramski, D.: Optical classification and characterization of marine particle assemblages within the western Arctic Ocean, Limnol. Oceanogr., 61, 1472–1494, 2016.

Nieke, B., Reuter, R., Heuermann, R., Wang, H., Babin, M. and Therriault, J. C.: Light absorption and fluorescence properties of chromophoric dissolved organic matter (CDOM), in the St. Lawrence Estuary (Case 2 waters), Cont. Shelf Res., 17, 235–252, 1997.

Pearson, R.K.: Mining imperfect data. Dealing with contamination and incomplete records. Society for Industrial and Applied Mathematics, 305 p. doi.org/10.1137/1.9780898717884, 2005.

Pegau, W.S., Gray, D., and Zaneveld, J.R.V.: Absorption and attenuation of visible and near-infrared light in water: Dependence on temperature and salinity, Appl. Opt., 36, 6035–6046, 1997.

15 Pope, R. M. and Fry, E. S.: Absorption spectrum (380–700 nm) of pure water. II. Integrating cavity measurements, Appl. Opt., 36, 8710–8723, 1997.

Poulet, S., Cossa, D. and Marty, J.-C.: Combined analyses of the size spectra and biochemical composition of particles in the St. Lawrence estuary, Mar. Ecol. Prog. Ser., 30, 205–214, 1986.

20 Poulton, S.W., and Raiswell R.: Chemical and physical characteristics of iron oxides in riverine and glacial meltwater sediments, Chem. Geol., 218, 203–221, 2005.

Ramalhosa, E., Pereira, E., Vale, C., Válega, M., Monterroso, and P., Duarte, A. C.: Mercury distribution in Douro estuary (Portugal), Mar. Poll. Bull. 50, 1218–1222, 2005.

25 Reynolds, R.A., Stramski, D., Wright, V.M., and Woźniak, S.B.: Measurements and characterization of particle size distributions in coastal waters, J. Geoph. Res., 115, doi:10.1029/2009JC005930, 2010.

Reynolds, R. A., Stramski, D. and Neukermans, G.: Optical backscattering by particles in Arctic seawater and relationships to particle mass concentration, size distribution, and bulk composition, Limnol. Oceanogr., 61, 1869–1890, 2016.

Risovic, D.: Two component model of the sea particle size distribution, Deep-Sea Res., Part I, 40, 1459–1473, 1993.

30 Röttgers, R., Schönfeld, W., Kipp, P.R., Doerffer, R.: Practical test of a point-source integrating cavity absorption meter: The performance of different collector assemblies, App. Opt., 44, 5549–5560, 2005.

Röttgers, R., McKee, D., and Woźniak, S. B.: Evaluation of scatter corrections for ac-9 absorption measurements in coastal waters, Methods Oceanogr., 7, 21–39, 2013.

Formatted: English (U.S.)

Formatted: English (U.S.)

Röttgers, R., Dupouy, C., Taylor, B. B., Bracher, A. and Woźniak, S. B.: Mass-specific light absorption coefficients of natural aquatic particles in the near-infrared spectral region, *Limnol. Oceanogr.*, 59, 1449–1460, 2014.

Slade, W.H., Boss, E. and Russo C.: Effects of particle aggregation and disaggregation on their inherent optical properties, *Opt. Exp.*, 19, 7945–7959, 2011.

5 Snyder, W., Arnone, R., Davis, C. O., Goode, W., Gould, R. W., Ladner, S., Lamela, G., Rhea, W. J., Stavn, R., Sydor, M. and Weidemann, A.: Optical scattering and backscattering by organic and inorganic particulates in U.S. coastal waters., *Appl. Opt.*, 47, 666–77, 2008.

Sokal, R. R. and Rohlf, F. J.: *Biometry: the principles of statistics in biological research*, 3rd ed., WH Freeman and Co, New York, NY., 1995.

10 Spearman, C.: The Proof and Measurement of Association between two things, *The Amer. J. of Psych.* , 15 , 1904.

Stavn, R. H. and Richter, S. J.: Biogeo-optics: particle optical properties and the partitioning of the spectral scattering coefficient of ocean waters., *Appl. Opt.*, 47, 2660–2679, 2008.

15 ~~Stavn, R.H., Rick H.J., and Falster and A.V.: Correcting the errors from variable sea salt retention and water of hydration in loss on ignition analysis: Implications for studies of estuarine and coastal waters, *Estuar. Coast. Shelf Sci.*, 81, 575–582, 2009.~~

Tremblay, L. and Gagné, J. P.: Distribution and biogeochemistry of sedimentary humic substances in the St. Lawrence Estuary and the Saguenay Fjord, Québec, *Org. Geochem.*, 38, 682–699, 2007.

Tremblay, L. and Gagné, J. P.: Organic matter distribution and reactivity in the waters of a large estuarine system, *Mar. Chem.*, 116, 1–12, 2009.

20 ~~Twardowski, M.S., Boss, E., Macdonald, J.B., Pegau, W.S., Barnard, A.H. and Zaneveld J.R.V.: A model for estimating bulk refractive index from the optical backscattering ratio and the implications for understanding particle composition in case I and case II waters, *J. Geophys. Res.*, 106, C7, 14,129-14,142, 2001.~~

25 ~~Tremblay, L., Kohl, S. D., Rice, J. A. and Gagné, J. P.: Effects of temperature, salinity, and dissolved humic substances on the sorption of polycyclic aromatic hydrocarbons to estuarine particles, *Mar. Chem.*, 96, 21–34, 2005.~~

Woźniak, S. B., Stramski, D., Stramska, M., Reynolds, R. A., Wright, V. M., Miksic, E. Y., Cichocka, M. and Cieplak, A. M.: Optical variability of seawater in relation to particle concentration, composition, and size distribution in the nearshore marine environment at Imperial Beach, California, *J. Geophys. Res. Ocean.*, 115, 1–19, 2010.

30 Xi, H., Larouche, P., Tang, S. and Michel, C.: Seasonal variability of light absorption properties and water optical constituents in Hudson Bay, Canada, *J. Geophys. Res. Ocean.*, 118, 3087–3102, 2013.

~~Xie, H., Aubry C., Bélanger S., and Song G.: The dynamics of absorption coefficients of CDOM and particles in the St. Lawrence estuarine system: Biogeochemical and physical implications, *Mar. Chem.*, 128-129, 44-56, 2012.~~

Yeats, P. A.: The distribution of trace metals in ocean waters, *Sci. Total Environ.*, 72, 131–149, 1988.

Yeats, P. A. and Bewers, J. M.: Trace metals in the waters of the Saguenay Fjord, *Can. J. Earth Sci.*, 13, 1319–1327, 1976.
Zaneveld, J.R.V., Kitchen, J.C., Moore, C.M.: The scattering correction error of the reflecting-tube absorption meters, *Ocean Optics XII*, J.S. Jaffe, Ed. International Society for Optical Engineering, SPIE proceedings, vol. 2258, 44-58, 1994.

5 Zhang, X., Hu, L., and He, M. X.: Scattering by pure seawater: Effect of salinity, *Opt. Exp.*, 17, 5698–5710, 2009.

Zhang, X., Huot, Y., Gray, D.J., Weidemann, A., and Rhea, W.J.: Biogeochemical origins of particles obtained from the inversion of the volume scattering function and spectral absorption in coastal waters, *Biogeosciences*, 10, 6029e6043, 2013.

Zhang, X., Stavn, R. H., Falster, A. U., Gray, D. and Gould, R. W.: New insight into particulate mineral and organic matter in coastal ocean waters through optical inversion, *Estuar. Coast. Res. Shelf Sci.*, 149, 1–12, 2014.

10 Zhang, X., Stavn, R.H., Falster, A.U., Rick, J.J., Gray, D. and R.W. Gould, Jr.: Size distributions of coastal ocean suspended particulate inorganic matter: Amorphous silica and clay minerals and their dynamics, *Estuar., Coast. and Shelf Sci.*, DOI: 10.1016/j.ecss.2017.03.025, 2017.

← Formatted: Tab stops: 1.9 cm, Left

15

20

25

30

Table 1. Summary of acronyms

Abbreviation	Definition	Unit
SLE	St. Lawrence Estuary	
UE	Upper Estuary	
SF	Saguenay Fjord	
LE	Lower Estuary	
$C_{SPM_{SPM}}$	Concentration of suspended particulate matter	$g m^{-3}$
F_{SPM}^i	Contribution of size fraction i to total mass of SPM	dimensionless
F_{SPM}^j	Contribution of chemical fraction j to total mass of SPM	dimensionless
NAP	Non-algal particulates	
CDOM	Chromophoric dissolved organic matter	
PIM	Particulate inorganic matter	$g m^{-3}$
POM	Particulate organic matter	$g m^{-3}$
λ	Light wavelength	nm
a_{SPM}	Absorption coefficient of SPM	m^{-1}
b_{SPM}	Scattering coefficient of SPM	m^{-1}
a_{SPM}^*	Mass-specific absorption coefficient of SPM	$m^2 g^{-1}$
b_{SPM}^*	Mass-specific scattering coefficient of SPM	$m^2 g^{-1}$
σ_a^j	Absorption cross section of SPM chemical fraction j	$m^2 g^{-1}$
σ_b^j	Scattering cross section of SPM chemical fraction j	$m^2 g^{-1}$

b_b^{**}	Backscattering efficiency	dimensionless
ξ^*	Differential Junge slope of particle size distribution Junge slope	Number of particulates per μm
D	Diameter of a volume-equivalent sphere at mid point of size class	μm
$V(D)$	Volume concentration at size class D	$\mu\text{L L}^{-1}$
$N(D)$	Particle number concentration at size class D	m^{-3}
$N'(D)$	Particle number density at size class D	$\text{m}^{-3} \mu\text{m}^{-1}$
γ	Spectral slope of particulate beam attenuation coefficient	nm^{-1}
S_{vis}	Spectral slope of mass-specific particulate absorption coefficient within the visible spectral range	nm^{-1}
BOI^{**}	Biogeo optical proxy for size distribution of SPM	dimensionless
BOI^{comp}	Biogeo optical proxy for chemical composition of SPM	dimensionless

← Formatted Table

Table 2. Summary of biogeochemical variables during June 2013. Acronyms UE, SF, LE are defined in Table 1. N is the number of samples per sub-region.

Sub-region	Fraction	Range	N
UE	$F_{SPM}^{<1\mu m}$	0.37–0.87	3
	$F_{SPM}^{0.2–0.4\mu m}$	0.04–0.08	3
	$F_{SPM}^{0.4–0.7\mu m}$	0.01–0.04	3
	$F_{SPM}^{0.7–10\mu m}$	0.77–0.89	3
	$F_{SPM}^{>10\mu m}$	0.05–0.17	3
SF	$F_{SPM}^{<1\mu m}$	0.49–0.66	5
	$F_{SPM}^{0.2–0.4\mu m}$	0.05–0.11	5
	$F_{SPM}^{0.4–0.7\mu m}$	0.01–0.14	5
	$F_{SPM}^{0.7–10\mu m}$	0.66–0.87	5
	$F_{SPM}^{>10\mu m}$	0.01–0.11	5
LE	$F_{SPM}^{<1\mu m}$	0.53–0.87	15
	$F_{SPM}^{0.2–0.4\mu m}$	0.02–0.27	15
	$F_{SPM}^{0.4–0.7\mu m}$	0.01–0.10	15
	$F_{SPM}^{0.7–10\mu m}$	0.48–0.93	15
	$F_{SPM}^{>10\mu m}$	0.03–0.15	15

← Formatted: Indent: First line: 1.27 cm

5

Table 3. Correlation Table 2. Particle size and chemical composition effects on mass-specific optical coefficients. Spearman rank

correlations for a_i^* and b_i^* are computed at a wavelength of 440 and 550 nm, respectively.

between IOPs of suspended particulates and SPM mass fractions. Each value is ρ_c with a statistical confidence level at 95 and 99% is symbolized with * and **, respectively. The number of observations per correlation is 23.

	λ	a_{SPM}	b_{SPM}
$F_{SPM}^{<1\mu m}$	440	0.21 **	0.59 **
	556	0.12 *	0.58 **
	665	0.02	0.56 **
	708	0.17 *	0.55 **
$F_{SPM}^{0.2-0.4\mu m}$	440	-0.01	0.66 **
	556	0.03	0.71 **
	665	-0.03	0.70 **
	708	-0.13 *	0.66 **
$F_{SPM}^{0.4-0.7\mu m}$	440	-0.06	0.28 **
	556	-0.05	0.35 **
	665	-0.09	0.31 **
	708	-0.20 **	0.27 **
$F_{SPM}^{0.7-10\mu m}$	440	0.12 *	-0.65 **
	556	-0.14 *	-0.67 **
	665	-0.17 *	-0.63 **
	708	-0.03	-0.57 **
$F_{SPM}^{>10\mu m}$	440	0.36 **	0.47 **
	556	0.35 *	0.39 **
	665	0.53 **	0.33 **
	708	0.41 **	0.28 **

Table 4. Particle size and chemical composition effects on mass-normalized IOPs. Spearman rank correlations for a_i^* and b_i^* are computed at a wavelength of 440 and 550 nm, respectively.

Mass-specific	ξ^*	F_{SPM}^{PIM}
<u>Optical fraction</u>		
<u> </u>		
$a_{0.2-0.4 \mu m}^*$	0.32 **	0.31 **
$a_{0.4-0.7 \mu m}^*$	0.28 **	0.50 **
$a_{0.7-10 \mu m}^*$	0.26 **	0.49 **
$a_{>10 \mu m}^*$	0.31 **	0.44 **
$b_{0.2-0.4 \mu m}^*$	0.15 *	-0.17 *
$b_{0.4-0.7 \mu m}^*$	0.05	-0.06
$b_{0.7-10 \mu m}^*$	0.23 **	0.42 **
$b_{>10 \mu m}^*$	0.37 **	0.26 **

← Formatted: Tab stops: 2.6 cm, Centered

Table 3. Correlation of optical proxies with particle size and composition. Spearman rank correlations based on 23 samples.**Table 5. Particle size and chemical composition effects on optical proxies. Statistic confidence levels of p_s -values are described in****Table 3.**

<u>Mass fraction of particulates</u>	<u>$\gamma_{BOF}^{size\downarrow}$</u>	<u>$SvisBOF^{size\downarrow}$</u>
F_{SPM}^{PIM}	<u>-0.34</u> -0.02	<u>-0.15</u> -0.16*
$F_{SPM}^{0.2-0.4 \mu m}$	<u>0.53*</u> -0.29 **	<u>0.49**</u> -0.03
$F_{SPM}^{0.4-0.7 \mu m}$	<u>-0.43*</u> -0.28**	<u>-0.49**</u> -0.35**
$F_{SPM}^{0.7-10 \mu m}$	<u>-0.38*</u> -0.27**	<u>-0.30*</u> -0.12*
$F_{SPM}^{>10 \mu m}$	<u>0.13</u> -0.04	<u>0.19</u> -0.40


Formatted Table

Table 6. Mass-normalized optical coefficients of suspended particulates for different littoral environments. Acronyms are defined in Table 1.

Table 4. Mass-specific optical coefficients of suspended particulates for different littoral environments. Acronyms are defined in Table 1.

Location	λ	a_{SPM}^*	b_{SPM}^*	σ_a^{POM}	σ_a^{PIM}	σ_b^{POM}	σ_b^{PIM}	$C_{SPM_{SPM}}$	References
UE	440	<u>0.01</u>	<u>0.01</u>						This study
		<u>0.250.01</u>	<u>1.060.01</u>	0.15	0.11	0.84	2.27	7.38 – 30.6	
		<u>2.68</u>	<u>2.74</u>						
	488	<u>0.01</u>	<u>0.01</u>						
		<u>0.140.01</u>	<u>0.970.01</u>	0.06	0.05	0.76	2.04		
		<u>0.99</u>	<u>2.70</u>						
	556	<u>0.01</u>	<u>0.01</u>						
		<u>0.060.01</u>	<u>0.860.01</u>	0.01	0.01	0.71	1.82		
		<u>0.32</u>	<u>2.55</u>						
	665	<u>0.01</u>	<u>0.01</u>						
		<u>0.020.01</u>	<u>0.730.01</u>	0.01	0.05	0.45	1.67		
		<u>0.15</u>	<u>4.75</u>						
	708	<u>0.01</u>	<u>0.01</u>						
		<u>0.0120.01</u>	<u>0.680.01</u>	0.01	0.02	0.11	1.31		
		<u>0.12</u>	<u>0.79</u>						
SF	440	<u>0.32</u>	<u>0.20</u>	1.71	0.86	1.78	0.94	2.28 – 3.68	
		<u>0.730.01</u>	<u>0.560.03</u>						

		<u>2.61</u>	<u>2.39</u>				
488	<u>0.17</u> -	<u>0.18</u> -					
	<u>0.39</u> <u>0.01</u>	<u>0.49</u> <u>0.05</u>	1.84	0.43	1.14	0.88	
	<u>4.76</u>	<u>4.76</u>					
556	<u>0.08</u> -	<u>0.15</u> -					
	<u>0.17</u> <u>0.01</u>	<u>0.42</u> <u>0.05</u>	0.85	0.17	0.45	0.56	
	<u>4.55</u>	<u>4.68</u>					
665	<u>0.02</u> -	<u>0.13</u> -					
	<u>0.04</u> <u>0.01</u>	<u>0.34</u> <u>0.01</u>	0.12	0.11	0.23	0.12	
	<u>0.70</u>	<u>0.68</u>					
708	<u>0.01</u> -	<u>0.12</u> -					
	<u>0.02</u> <u>0.01</u>	<u>0.31</u> <u>0.01</u>	0.01	0.01	0.12	0.04	
	<u>0.44</u>	<u>0.49</u>					
LE	440	<u>0.03</u> -	<u>0.04</u> -				
	<u>0.07</u> <u>0.01</u>	<u>0.22</u> <u>0.01</u>	0.07	0.02	2.64	2.04	2.72 - 25.7
	<u>4.95</u>	<u>2.17</u>					
488	<u>0.02</u> -	<u>0.04</u> -					
	<u>0.04</u> <u>0.01</u>	<u>0.21</u> <u>0.01</u>	0.03	0.01	2.13	1.88	
	<u>4.24</u>	<u>2.06</u>					
556	<u>0.01</u> -	<u>0.04</u> -					
	<u>0.02</u> <u>0.01</u>	<u>0.19</u> <u>0.01</u>	0.01	0.01	1.88	1.36	
	<u>4.18</u>	<u>4.38</u>					
665	<u>0.003</u> -	<u>0.04</u> -					
	<u>0.006</u> <u>0.01</u>	<u>0.18</u> <u>0.01</u>	0.02	0.01	1.42	0.89	
	<u>4.04</u>	<u>4.03</u>					
708	<u>0.015</u> -	<u>0.04</u> -	0.02	0.01	0.98	0.67	
	<u>0.02</u> <u>0.01</u>	<u>0.17</u> <u>0.01</u>					

		0.88	0.88			
Elber River,	650	0.001 0.020	–	0.5-10	Röttgers et al. (2014)	
German Bight,	750	0.001 0.019	–			
Baltic Sea, New Caledonia lagoon	850	0.001 0.014	–			
Monterey Bay, US	532		0.46 – 2.54	1.23–3.39 0.08 – 0.77 0.11 – 2.37	Zhang et al. (2014)	
Mobile Bay, US	532		0.40 – 1.78	0.35–3.85 0.27 – 0.79 0.26 – 7.36		
Hudson Bay, Canada	675	0.001 – 0.12		0.2 – 2.5	Xi et al. (2013)	
Mississippi River, US	450	0.02 – 0.11		7-25	Bowers and Binding (2006)	
	550	0.017 – 0.06				
	650	0.012–0.035				

700 0.01 – 0.025

Mobile Bay,	440	0.44 – 1.95		0.01-1.91	0.36 – 0.80	0.23-25.32	Stavn and Richter (2008)
Southwest Pass, US	488	0.41 – 1.89		0.01-1.82	0.36-0.73		
	550	0.40 – 1.80		0.01-1.65	0.33-0.70		
	676	0.36 – 1.63		0.04-1.48	0.34-0.63		
	715	0.34 – 1.61		0.02-1.39	0.33-0.58		
Coast of New Jersey,	440		0.23 – 0.08 – 0.59 0.17	0.7 – 5.1	0.3 – 1.3	0.44 – 6.6	Snyder et al. (2008)
Monterey Bay,	488		0.18 – 0.07 – 0.39 0.13	0.65 – 4.8	0.4 – 1.6		
Great Bay	556		0.13 – 0.05 – 0.21 0.08	0.4 – 4.3	0.5 – 1.8		
<u>Mobile Bay</u>	<u>0.05 ± 0.01</u> <u>(arithmetic</u> <u>mean ±</u> <u>standard</u> <u>deviation)</u>		0.09 – 0.05 – 0.11 0.06	0.35 – 3.8	0.4 – 1.7		
	665						
	708		0.02 – 0.01 – 0.03 0.02	0.4-3.9	0.3-1.7		

Irish sea, UK 665 0.08 – 0.45 0.01 – 0.02 0.47 – 0.49 1.9 – 26.5 Binding et al. (2005)

Irish sea, UK 443 $\frac{0.062}{0.013} \pm$ 0.17 – 0.19 0.05 – 0.06 0.25 – 0.27 1.6 – 50 Bowers and Binding (2006)

490 0.20 – 0.22 0.03 – 0.04 0.33 – 0.37

555 0.20 – 0.24 0.03 – 0.03 0.37 – 0.39

665 0.14 – 0.15 0.02 – 0.03 0.27 – 0.29

English channel, UK 550 0.62 – 1.04 0.01 – 72.8

Coast off Europe and French 676 0.63 – 2.07 0.12 – 1.83 1.2 – 82.4 Neukermans et al. (2012)

Guyana

Guyana coast, Scheldt 440 0.02 – 0.12 0.37 – 0.89 30 – 120 Dogliotti et al. (2015)

River, Rio
de la Plata
Estuary

Elbe
Estuary, Germany
555 0.05 – 0.07 0.35 – 0.47
715 0.01 – 0.03 0.32 – 0.44

Gironde
Estuary, France
555 0.02 – 0.06 0.28 – 0.50
715 0.01 – 0.02 0.27 – 0.45

Coastal Louisiana and lower Atchafalaya and Mississippi
440 0.056 ± 0.012
(0.05-0.065)

Rivers
488 0.035-0.05
556 0.25-0.35
665 0.125-0.02

West of Mississippi Delta Imperial Beach
443 0.012-0.079
0.03-0.1 0.1-1.2

Doxaran et al. (2009)
73.5 – 294.2

21.9 – 344.1

Estapa et al. (2012)

← Formatted Table

D'Sa et al. (2006)
3-90

Wozniak et

<u>California</u>	<u>440</u>	<u>al. (2010)</u>
<u>488</u>	<u>0.02-0.08</u>	<u>0.18-0.9</u>
<u>556</u>	<u>0.01-0.03</u>	<u>0.2-0.9</u>
<u>665</u>	<u>0.004-0.02</u>	<u>0.2-0.8</u>
<u>708</u>	<u>0.001-0.02</u>	<u>0.2-0.8</u>

Appendix A

Table A1. Correlations between γ , F_{SPM}^{PBM} , and IOPs of SPM size fractions. First, second, third and fourth p -values correspond to the wavelengths 440, 556, 665 and 708 nm, respectively.

γ	F_{SPM}^{PBM}
$a_{0.2-0.4 \mu m}$	<u>-0.17*</u> , <u>0.21**</u> , <u>0.01</u> , <u>0.01</u>
$a_{0.4-0.7 \mu m}$	<u>0.31**</u> , <u>0.07</u> , <u>0.33**</u> , <u>0.20*</u>
$a_{0.7-1.0 \mu m}$	<u>0.07</u> , <u>0.31**</u> , <u>0.07</u> , <u>0.11*</u>
$a_{>10 \mu m}$	<u>0.21**</u> , <u>0.30**</u> , <u>0.30**</u> , <u>0.08</u>
$b_{0.2-0.4 \mu m}$	<u>-0.29**</u> , <u>0.26**</u> , <u>0.30**</u> , <u>0.25**</u>
$b_{0.4-0.7 \mu m}$	<u>-0.21**</u> , <u>0.18*</u> , <u>0.21**</u> , <u>0.16*</u>
$b_{0.7-1.0 \mu m}$	<u>0.50*</u> , <u>0.16*</u> , <u>0.50**</u> , <u>0.41**</u>
$b_{>10 \mu m}$	<u>0.34**</u> , <u>0.05</u> , <u>0.24**</u> , <u>0.19*</u>

Table A2. Correlations between size and chemical fractions of SPM.

	F_{SPM}^{PM}
$F_{SPM}^{0.2-0.4\mu m}$	0.27 **
$F_{SPM}^{0.4-0.7\mu m}$	0.15 *
$F_{SPM}^{0.7-10\mu m}$	0.08
$F_{SPM}^{>10\mu m}$	-0.27 **

Table A3. Correlations between chlorophyll a concentration and γ . N is the number of observations.

	γ	N
UE	-0.08	3
SF	0.62 **	4
LE	-0.45 **	14

5

10

15

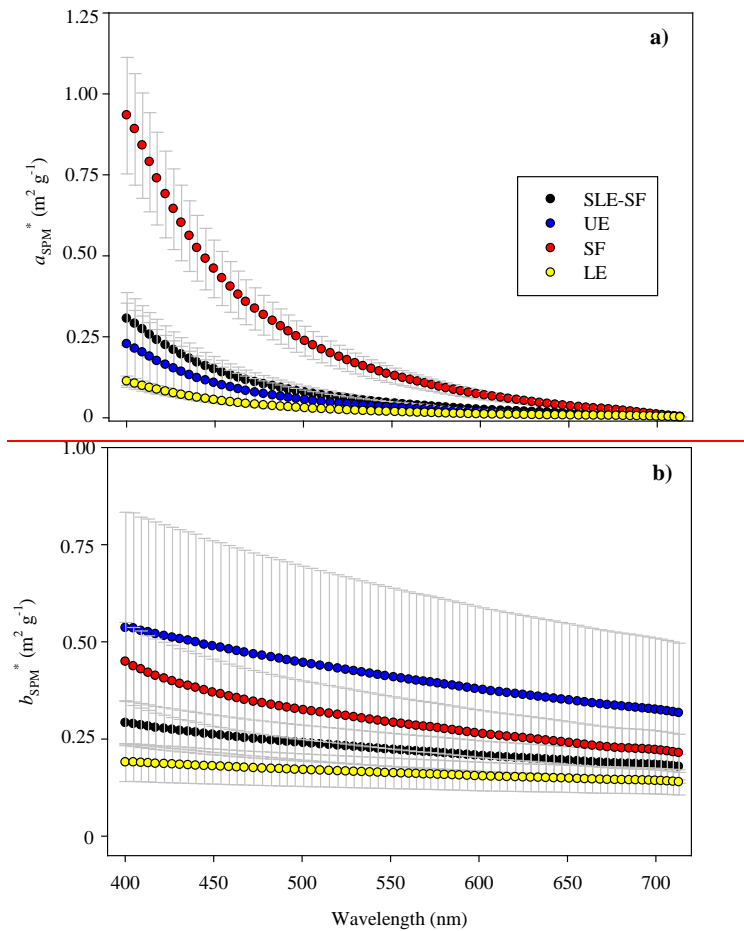


Fig A1

Figure captions

Figure 1. Study area. UE (green triangles), LE (blue rectangles) and SF (red circles). GSL is the Gulf of St. Lawrence.

Figure 2. Spectral variation of mass-normalized optical coefficients of SPM. (a) particulate absorption at $\lambda = 440$ nm, (b) particulate scattering at $\lambda = 550$ nm. Each bar corresponds to the arithmetic average over the whole study area; uncertainty bars 5 symbolize ± 2 standard errors.

Figure 3. Sub-regional variation of mass-normalized optical coefficients of SPM. (a) particulate absorption at $\lambda = 440$ nm, (b) particulate scattering at $\lambda = 550$ nm.

Figure A1. Spectral variation of mass-specific absorption and scattering coefficients of suspended particulate matter. (a) absorption, (b) scattering. Error bars represent 1 standard error.

Figure 3. Spectral variation of mass-specific absorption coefficients for different size classes of suspended particulates. (a) 0.2-0.4 μm , (b) 0.4-0.7 μm , (c) 0.7-10 μm and (d) $>10 \mu\text{m}$. Curves presenting negative values at some wavelengths are not depicted. SF (black line), UE (red line) and LE (blue line).

Figure 4. Spectral variation of mass-specific scattering coefficients for different size classes of suspended particulates. (a) 0.2-0.4 μm , (b) 0.4-0.7 μm , (c) 0.7-10 μm and (d) $>10 \mu\text{m}$. Curves presenting negative values at some wavelengths are not depicted. SF 15 (black line), UE (red line) and LE (blue line).

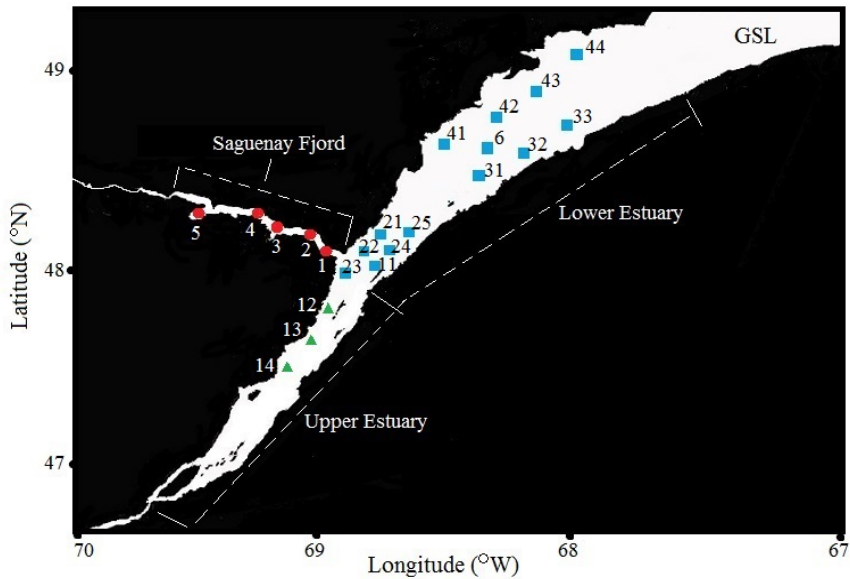
Figure 5. Comparison of mass-normalized optical coefficients for different SPM fractions. (a) mass-specific (left-axis) and true optical cross section (right-axis) for particulate absorption, (b) idem as (a) but for particulate scattering. Each bar is the arithmetic average ± 2 standard errors as computed by using the whole dataset.

Figure 6. Sub-regional variation of mass-specific optical coefficients of SPM. (a) particulate absorption at $\lambda = 440$ nm, (b) 20 particulate scattering at $\lambda = 550$ nm. Each bar is the arithmetic average ± 2 standard errors as computed for each spatial domain.

5

10

15



5

fig. 1

10

15

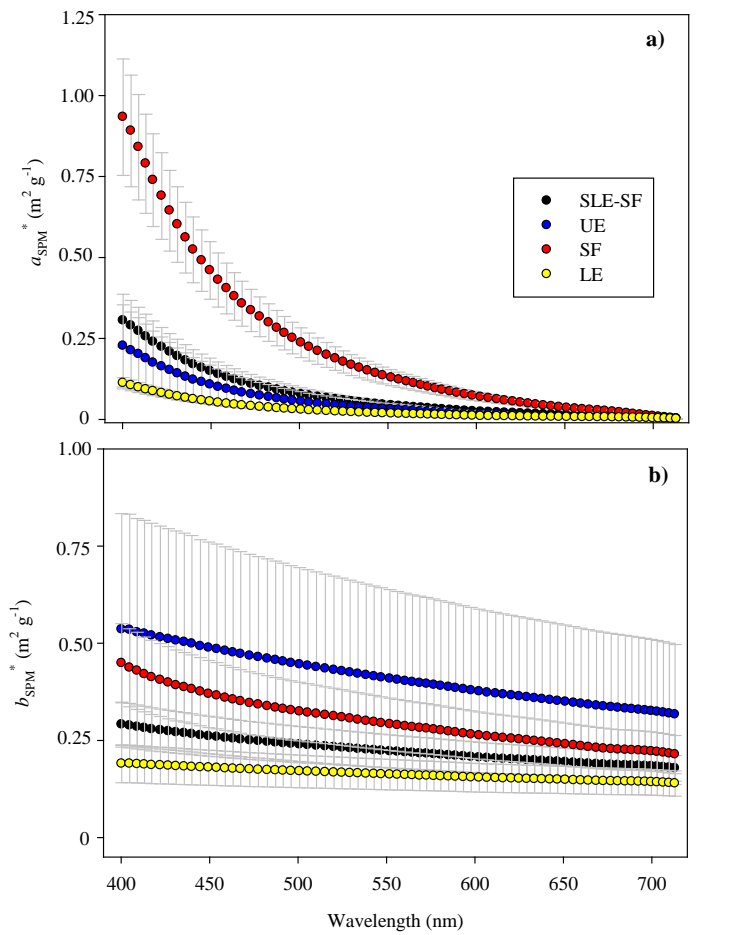


Fig. 2

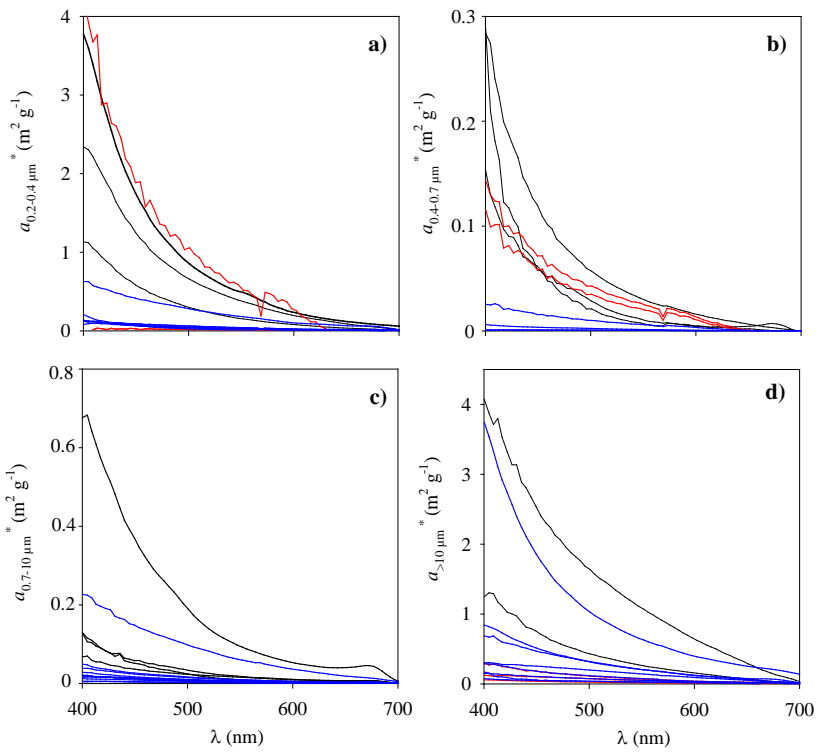


Fig. 3

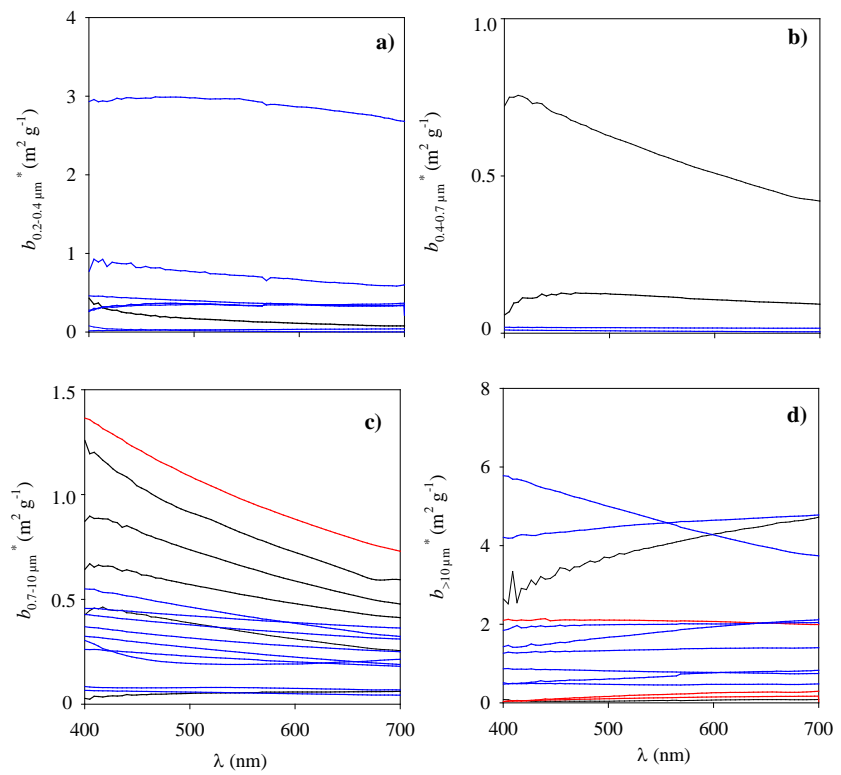


Fig. 4

